An edited version of this paper was published by AGU. Copyright 2008 American Geophysical Union: **Eck, T. F. et al. (2008), Spatial and temporal variability of column-integrated aerosol optical properties in the southern Arabian Gulf and United Arab Emirates in summer, J. Geophys. Res., 113, D01204, doi:10.1029/2007JD008944.**

Spatial and Temporal Variability of Column Integrated Aerosol Optical Properties in the Southern Arabian Gulf and United Arab Emirates in Summer

T.F. Eck[1,2], B. N. Holben[2], J. S. Reid[3], A. Sinyuk[4,2], O. Dubovik[5], A. Smirnov[1,2], D. Giles[4,2], O'Neill[6], N.T., S.-C. Tsay[2], Q. Ji[7,2], A. Al Mandoos[8], M. Ramzan Khan[8], E. A. Reid[3], J. S. Schafer[4,2], M. Sorokine[4,2], W. Newcomb[4,2], and I. Slutsker[4,2]

[1]Goddard Earth Sciences and Technology Center, University of Maryland-Baltimore County, Baltimore, Maryland, USA
[2]NASA Goddard Space Flight Center, Greenbelt, Maryland, USA
[3]Naval Research Laboratory, Monterey, California, USA
[4]Science Systems and Applications, Inc., Lanham, Maryland, USA
[5]Laboratoire d'Optique Atmospherique, Universite´ de Lille, Villeneuve d'Ascq, France
[6]CARTEL, Universite de Sherbrooke, Sherbrooke, Quebec, Canada
[7]University of Maryland, College Park, Maryland, USA
[8]Dept. of Atmospheric Studies, Ministry of Presidential Affairs, United Arab Emirates

Abstract

A mesoscale network of 14 AERONET sunphotometers was established in the UAE and adjacent Arabian Gulf waters during August through September 2004 as a component of the United Arab Emirates Unified Aerosol Experiment (UAE^2). These measurements allowed for spatial, temporal and spectral characterization of the complex aerosol mixtures present in this

environment where coarse mode desert dust aerosols often mix with fine mode pollution aerosols produced by petroleum extraction and processing activity. Aerosol loading was relatively high with two-month averages of aerosol optical depth (AOD) at 500 nm (τ_{a500}) ranging from 0.40 to 0.53. A higher fine mode fraction of AOD was observed over Arabian Gulf island sites with Angstrom exponent at 440-870 nm ($\alpha_{440\text{-}870}$) of 0.77 as compared to an average of 0.64 over coastal sites and 0.50-0.57 at inland desert sites. Most fine mode pollution originates from island or coastal industrial and petroleum processing facilities thus causing this $\alpha_{440\text{-}870}$ spatial distribution. Comparison of AOD and $\alpha_{440\text{-}870}$ between a site located on the Arabian Gulf versus a site on the Gulf of Oman coast shows high correlation between the two suggesting that the mountain range separating these sites does not significantly block aerosol advection. This is consistent with the comparison of AOD from a mountain ridge site to a desert floor elevation site, which indicates that only ~25% of the aerosol is located in the lowest 800 meter layer; as a result most of the aerosol is above the adjacent mountain range altitude. AOD is correlated with total column integrated water vapor (r^2~0.45-0.65) for both fine and coarse mode dominated aerosol mixtures, suggesting that advection from major aerosol sources is often associated with aerosol transport over the humid Arabian Gulf. During pollution events with high Angstrom exponent ($\alpha_{440\text{-}870}$>1) the retrieved fine mode radius was larger over a Gulf island site than a desert site probably due to hygroscopic growth over the humid marine environment. For these same pollution dominated cases, single scattering albedo (ω_o) at all wavelengths is ~0.03 higher (less absorption) over the marine environment than over the desert, also consistent with aerosol humidification growth. At an inland desert location, the single scattering albedo at 440 nm remained relatively constant as Angstrom exponent varied since the fine mode pollution and coarse mode dust are both strong absorbers at short wavelengths. However, at longer

wavelengths (675-1020 nm) the dust is much less absorbing than the pollution resulting in ω_o that were 0.04-0.05 higher for dust cases with $\alpha_{440\text{-}870}<0.4$ as compared to pollution dominated cases where $\alpha_{440\text{-}870}>1.0$. At an Arabian Gulf coast site ~60 km from Abu Dhabi the afternoon AERONET retrievals of ω_o are ~0.03 higher than the morning values, which is in agreement with in situ measured trends at the surface, although the in situ data show 0.05 higher in the afternoon. These observations are consistent with the land/sea breeze diurnal cycle with more absorbing pollution increasing during the night and less absorbing aerosol advected inland during the daytime sea breeze flow. Other AERONET sites located farther from major pollution sources or distant from the coastal zone do not show any significant diurnal variation in ω_o however.

1. Introduction

In the summer of 2004 the UAE Unified Aerosol Experiment (UAE^2) field campaign was conducted in the United Arab Emirates and over the adjacent Arabian Gulf and Gulf of Oman waters [*Reid et al.*, 2007a]. The focus areas of this field campaign included the characterization of fundamental physical and optical properties of atmospheric aerosol particles, the interaction of the regional/local meteorology with the aerosol radiative impacts, and the remote sensing of heterogeneous aerosol properties over the water and bright desert surfaces. Over sixty scientists and engineers from several countries participated in ground-based and airborne data collection and analysis.

The aerosol environment in this region is extraordinarily complex. The geographical location of the UAE includes strong regional desert dust sources of predominately coarse mode size particles and complex shape, as well as strong fine mode pollution particle sources from petroleum extraction and processing facilities. This variability of atmospheric particle type, size, and shape in conjunction with highly variable regional meteorology results in some days that are

dominated by large particle desert dust, some dominated by fine particle pollution, and many days that are a mixture of aerosol types. Additionally, the high spectral reflectance of most arid land surfaces in the region results in difficulty in remote sensing of aerosol optical properties from satellites.

A major component of the UAE^2 field campaign was the establishment of 14 AErosol RObotic NETwork (AERONET) sun photometer sites in various environments including Arabian Gulf islands, coastal locations, inland deserts, and a mountain ridge top. This measurement campaign provided the highest density mesoscale network of sites ever established by AERONET, and allowed for regional study of the temporal and spatial variation of effective total column integrated optical properties in addition to more rigorous than usual characterization of both satellite and ground based remote sensing retrievals. Here we investigate the spatial distribution and temporal dynamics of the total column atmospheric aerosol optical depth (AOD), and retrieved aerosol size distributions and single scattering albedo. AERONET retrievals yield the total column radiatively effective size distributions and single scattering albedos. This study attempts to quantify the dynamics of aerosol optical properties in the late summer season in the UAE. Information on the variability of these spectrally variable optical parameters is presented to aid in the refinement and validation of remote sensing retrievals of aerosol optical depth and properties and in determining the potential climatic effects of aerosol perturbations to the regional radiation budget. Additionally, by using the prevalence of open desert, coastal, and open water sites and range of aerosol types and mixtures we examine the characteristics of the new AERONET version 2 retrievals.

2. Instrumentation, Study Sites and Techniques

2.1 AERONET Instrumentation

98 The CIMEL Electronique CE-318 sun-sky radiometer measurements reported in this paper were
99 made with instruments that are a part of the AERONET global network. These instruments are
100 described in detail in *Holben et al.* [1998], however a brief description will be given here. The
101 automatic tracking Sun and sky scanning radiometers made direct Sun measurements with a 1.2^0
102 full field of view every 15 minutes at 340, 380, 440, 500, 675, 870, 940, and 1020 nm (nominal
103 wavelengths). Additionally 4 sites (Dalma, Dhadnah, SMART and MAARCO) had the new
104 extended wavelength version of the CIMEL with the 1640 nm channel added to the 8 standard
105 wavelengths (we do not analyze the 1640 nm data in this paper as this is the topic of another
106 investigation (*O'Neill et al.*, 2007)). For the SMART_POL site the polarized version of the
107 CIMEL made measurements at 440, 675, 870, 940, and 1020 nm, in addition to three polarized
108 channels at 870 nm (the polarized channels were also not analyzed in this study). The direct sun
109 measurements take ~8 seconds to scan all 8 wavelengths, with a motor driven filter wheel
110 positioning each filter in front of the detector. These solar extinction measurements are then used
111 to compute aerosol optical depth at each wavelength except for the 940 nm channel, which is
112 used to retrieve total columnar (or precipitable) water vapor in centimeters. The filters utilized in
113 these instruments were ion assisted deposition interference filters with bandpass (full width at
114 half maximum) of 10 nm, except for the 340 and 380 nm channels at 2 nm. Calibration of field
115 instruments was performed by a transfer of calibration from reference instruments that were
116 calibrated by the Langley plot technique at Mauna Loa Observatory (MLO), Hawaii. The inter-
117 calibration of field instruments was performed both pre- and post- deployment at Goddard Space
118 Flight Center (GSFC) and a linear change in calibration with time was assumed in the
119 interpolation between the two calibrations. The uncertainty, due primarily to calibration
120 uncertainty is ~0.010-0.021 in computed τ_a for field instruments (which is spectrally dependent

121 with the higher errors in the UV; *Eck et al.* [1999]). *Schmid et al*. [1999] compared τ_a values
122 derived from 4 different solar radiometers (including an AERONET sun-sky radiometer)
123 operating simultaneously together in a field experiment and found that the τ_a values from 380 to
124 1020 nm agreed to within 0.015 (rms), which is similar to our estimated level of uncertainty in τ_a
125 retrieval for field instruments. The spectral aerosol optical depth data have been screened for
126 clouds following the methodology of *Smirnov et al.* [2000], which relies on the greater temporal
127 variance of cloud optical depth versus aerosol optical depth. The sky radiances measured by the
128 sun/sky radiometers are calibrated versus the 2-meter integrating sphere at the NASA Goddard
129 Space Flight Center, to an absolute accuracy of ~5% or less.

130 **2.2 Study Region and Sites**

131 Figure 1 presents a map of the UAE and Arabian Gulf showing the 14 AERONET sites that
132 were deployed for the UAE^2 field campaign. We analyzed data from 12 of these sites in the
133 current study, excluding the Abu Al Bukhoosh site since it was only established on September
134 20, 2004, toward the end of the campaign period, and also excluding the Dhabi site since there
135 were multiple changes in instruments (and some instrument problems). The distribution of
136 analyzed sites covers all of the major environments in the region including Gulf islands (Dalma
137 and Sir Bu Nuair), coastal sites (Al Qlaa, MAARCO, Umm Al Quwain, and Dhadnah), inland
138 desert sites (Mezaira, Hamim, and SMART), coastal plain/inland sites (Saih Salam and Al
139 Khaznah), and a mountain ridge site (Jabal Hafeet). This dense distribution of sites is unique in
140 the history of AERONET and it allows for the study of differences in aerosol properties due to
141 relative humidity differences (very humid over the Gulf versus very dry over the desert), vertical
142 distribution of aerosol (mountain site at Jabal Hafeet versus nearby desert site, SMART at Al
143 Ain), and differences between coastal sites located on the Arabian Gulf versus the Gulf of Oman

144 (Umm Al Quwain versus Dhadnah). In order to help perform primary validation of new over-
145 desert satellite optical depth algorithms (such as Deep Blue, Hsu et al., [2007]), sites were also
146 chosen based on regional surface albedo, with sites bordering dramatic shifts in surface
147 properties receiving a high priority for data collection and analysis (such as Hamim and Mezeria)
148 Two placements during the UAE campaign were associated with mobile laboratory super
149 sites: the Naval Research Laboratory (NRL) Mobile Atmospheric Aerosols and Radiation
150 Characterization Observatory (MAARCO; *Reid et al.,* [2007b]); and the NASA Goddard SFC
151 Surface-sensing Measurements for Atmospheric Radiative Transfer (SMART; http://smart-
152 commit.gsfc.nasa.gov). The MAARCO site was located on the coast ~60 km northeast of Abu
153 Dhabi and housed an extensive set of instruments for meteorological measurements, in situ
154 aerosol sampling, and aerosol remote sensing. The SMART trailer, with a complete set of
155 surface based radiation and remote sensing instrumentation, was established at the inland desert
156 site located at the Al Ain airport.

157 **2.3 Inversion Methodology**

158 The CIMEL sky radiance measurements in the almucantar geometry (fixed elevation angle equal
159 to solar elevation and a full 360^0 azimuthal sweep) at 440, 675, 870, and 1020 nm (nominal
160 wavelengths) in conjunction with the direct sun measured τ_a at these same wavelengths were
161 used to retrieve optical equivalent aerosol size distributions and refractive indices. Using this
162 microphysical information the spectral dependence of single scattering albedo (ω_o) is calculated.
163 The algorithm of *Dubovik and King* [2000] with enhancements detailed in *Dubovik et al.* [2006]
164 was utilized in these retrievals, known as Version 2 AERONET retrievals. Level 2 quality
165 assured retrievals [*Holben et al.*, 2006] are presented in this paper. In the Version 2 algorithm,
166 particle shape is portioned into two components: spherical and non-spherical. The spherical

component is modeled as an ensemble of polydisperse homogeneous spheres, while the non-spherical component is modeled as a mixture of polydisperse randomly oriented homogeneous spheroids with a fixed aspect ratio distribution. The spheroid aspect ratio distribution utilized is the one obtained from fitting [see Dubovik et al. 2006] of the phase matrix measurements of feldspar by Volten et al. [2001], and it is used in all AERONET retrievals (regardless of the mineral type of the dust). As discussed in Dubovik et al. 2006, this model is capable of reproducing the main features of non-spherical dust light scattering properties required for the fitting of observations. In addition, the fitting error of this algorithm to AERONET measurements of dust is small (comparable to measurement accuracy), indicating that the model works rather well in all cases. Use of only one model in AERONET dust retrievals is supported by the fact that AERONET radiometric measurements are not sensitive to details of the aspect ratio distribution [see Dubovik et al. 2006]. For example, as discussed by Dubovik et al. [2006], simple mixtures of spheroids with relatively constant aspect ratios ranging from 1.5 to 3 are able to reproduce the main features of non-spherical dust scattering. Information on the morphology of ambient mineral dust is very difficult to collect and these measurements were not made during the UAE^2 campaign. The Version 2 AERONET algorithm determines the percentage of spherical particles required to give the best fit to the measured spectral sky radiance angular distribution.

Another improvement made in the Version 2 almucantar retrievals is the specification of more accurate surface reflectance as an input boundary condition to the retrieval. Large errors in prescribed surface reflectance can affect the accuracy of retrieved aerosol parameters including single scattering albedo [*Sinyuk et al.,* 2007]. In Version 1 the reflectance was assumed to be Lambertian and invariant geographically, with reflectance values of 0.03, 0.06, 0.20, and 0.20 for

190 the 440 nm, 675 nm, 870, and 1020 nm wavelengths, respectively. Bright soil and sand surfaces
191 of the arid environments in the UAE have much higher spectral reflectance (and consequently
192 result in greater sky brightness) than the values assumed in Version 1 retrievals. In Version 2,
193 bidirectional reflectance distribution function (BRDF) models are utilized that allow for dynamic
194 reflectance as a function of solar zenith angle over land and water. Over the ocean, the *Cox and*
195 *Munk* [1954] model approximates the water BRDF as a function of wind speed (wind speed data
196 are from NCEP/NCAR Reanalysis; *Kalnay et al.*, 1996) and over the land the Li-Ross model of
197 *Lucht and Roujean* [2000] is applied. The land BRDF parameters are adopted from MODIS
198 generic ecosystem type models and mixed by the ecosystem map of *Moody et al.* [2005].
199 Geographically and seasonally (16-day interval) varying surface albedo estimates from *Moody et*
200 *al.* [2005)], based on MODIS atmospherically corrected data, were used to vary the magnitude of
201 the BRDF values. The MODIS albedo data from a 5 km radius centered on each site are
202 averaged. In Table 1 the spectral albedo values computed from Version 2 BRDF for the solar
203 zenith angle range 50^0 to 77^0 are given for an inland sandy desert site (Hamim), an Arabian Gulf
204 island site (Sir Bu Nuair – only ~15% land), and a coastal site (Al Qlaa, ~50% land). Obviously,
205 the table shows significant variation in surface albedo in the study region and also significant
206 departure from the Version 1 assumption for all sites.
207 Almucantar sky radiance measurements were made at optical airmasses of 4, 3, 2, and 1.7 in
208 the morning and afternoon, and once per hour in between. In order to ensure sky radiance data
209 over a wide range of scattering angles, only almucantar scans at solar zenith angles greater than
210 50 degrees are analyzed and presented here. To eliminate cloud contamination from the
211 almucantar directional sky radiance data we require the radiances to be symmetrical on both
212 sides of the sun at equal scattering angles. The stable performance of the inversion algorithm was

illustrated in sensitivity studies performed by *Dubovik et al.* [2000] where the perturbations of the inversion resulting from random errors, possible instrument offsets and known uncertainties in the atmospheric radiation model were analyzed. Retrieval tests using known size distributions demonstrated successful retrievals of mode radii and the relative magnitude of modes for various types of bimodal size distributions such as those dominated by a sub-micron accumulation mode or distributions dominated by coarse mode aerosols.

3. Results and Discussion

3.1 Spatial, Temporal and Spectral Variability of AOD

3.1.1 Temporal and Spatial Variability of Daily Average AOD and Angstrom Exponent

A time series of daily average AOD at 500 nm from August 9 though October 2, 2004 for four AERONET station sites (Sir Bu Nuair, Umm Al Quwain, Saih Salam, and SMART) in the UAE is shown in Figure 2a. These sites are a representative sample over various environments, including, respectively, an Arabian Gulf island site, a coastal site, a site on the coastal plain, and an inland site. It is noted that the 500 nm AOD is typically quite high at all sites in this season, exceeding ~0.4 on most days with maximum values of ~1.0 and minimum of ~0.15. The temporal variability patterns are similar for these sites on most days suggesting that regional scale aerosol variation often dominates over local effects. Table 2 shows averages of the AOD(500 nm), Angstrom Exponent (440-870 nm), and total columnar water vapor for the entire time interval for eight sites in the UAE. For six of the eight sites in Table 2 there are 55 daily averages (no missing days), while the other 2 sites have 53 and 54 daily averages that are utilized to compute the August 9 –October 2 mean. This high data collection rate results from the very low incidence of cloud cover in much of the UAE during the summer season. Other sites are not included in Table 2 since there were too many missing days over this time interval, thus negating

direct comparisons. The ~2 month average AOD for these eight sites ranges from 0.40 to 0.53, with all inland desert sites having lower AOD (0.40 to 0.43), while most island and coastal sites have higher values (0.48 to 0.53). However the island site of Dalma has relatively low AOD (0.44) indicating that the relative location to the Arabian Gulf is not in itself an accurate predictor of aerosol loading. Location relative to upwind aerosol sources coupled with the sometimes complicated meso-scale flows are likely key reasons for regional variability. It is interesting that the total columnar water vapor over Dalma is similar to that over the inland desert sites, further suggesting complex variation in regional scale circulation. The proximity of Dalma to the Qatar peninsula may influence the local boundary layer circulation.

The time series of the daily average Angstrom wavelength exponent (computed from 440 to 870 nm AOD data) for the same sites and dates is shown in Figure 2b. It is noted in this figure that the Angstrom exponent is quite variable, ranging from ~0.2 to ~1.6, as a result of some days being dominated by strong desert dust events and some days where pollution aerosol is predominant although most days exhibit a mixture of aerosol types. At these four UAE sites, the Angstrom exponent averages 0.77 for the Gulf island site of Sir Bu Nuair, 0.64 for the coastal site of Umm Al Quwain, and 0.55 and 0.50 at the inland desert sites of Saih Salam and SMART, respectively. Therefore the higher Angstrom exponent values for the Gulf island and coastal sites indicate that fine mode pollution particles are present in greater concentrations there than at inland desert sites. Table 2 shows a strong relationship between geographical location and the average Angstrom exponents, with both Gulf island sites having $\alpha = 0.77$, both sites on the coast having 0.64 and inland desert sites ranging from 0.50 to 0.57. Higher Angstrom exponents at sites in or bordering the Arabian Gulf are likely due to the sources of fine mode particle pollution originating from petroleum industry operations at offshore platforms, on islands, and on the

coast. These fine mode aerosol particles are dominated by sulfates [*Ross et al.*, 2007] that are very hygroscopic; therefore they grow in size in high humidity environments, which thereby increases the fine mode scattering optical depth. The slightly higher α at Hamim and Mezaira compared to the SMART site may result from the emissions of a large oil processing complex located approximately midway between the Gulf coast and the Hamim and Mezaira sites.

3.1.2 Diurnal Variability of AOD and Angstrom Exponent

As discussed in *Eager et al.*, [2007] the Southern Arabian Gulf is strongly influenced by regional sea and land breeze circulations. The impact of these circulations can be seen in Figure 3, where the mean diurnal variability of AOD and Angstrom exponent expressed as the departure from the daily mean versus the local time of day is presented. At each site the means for each day are computed and then the absolute departure from that is computed for each observation, and averaged in hourly bins (similar to *Smirnov et al.* (2002a)). The departures from daily mean for each hour are then averaged over an approximately two month period, August through September for most sites, although for Al Qlaa the time period was June 24 – Aug 24 since the instrument was removed from the site on Aug 25. For most sites the departures from the daily mean do not exceed 0.02 for most hours (change of <5%), and with no strong trend over the daily cycle.

Two sites that do show similar coherent diurnal trends are MAARCO and Sir Bu Nuair. At both of these locations the AOD is maximum in the early morning and then it decreases slowly at first through the morning and mid-day and then more rapidly in the afternoon. The average minimum to maximum range of AOD at these sites is ~0.07. This pattern is explained by the diurnal land-sea breeze circulations [*Eager et al.*, 2007]. During morning hours the coastal UAE experiences offshore flow. Dust generated from the previous day is carried out towards the coast

and the Gulf, increasing AOD and decreasing the Angstrom exponent. By mid day, flows reverse to onshore, with a lesser burden of dust (and consequently AOD) and occasional increases of fine mode particles from offshore petroleum operations.

Another site that exhibits a similarly large range of average AOD over the diurnal cycle is the SMART site with a minimum in mid morning through mid-day and a maximum in late afternoon. This scenario is also explained by the land and sea-breeze circulations. The sea breeze front usually arrives at ~10:00-11:00 LST bringing with it a ~2-3 m s^{-1} increase in wind speed. These sea breeze winds often reached the interior desert by 14:00-15:00 LST and frequently moved as far inland as the SMART site and sometimes to the Hamim site, bringing with them dust produced over the UAE desert. A second phenomenon, the haboob, or strong surface winds (a result of thunderstorm outflow) was also frequently observed over the interior desert sites during the mission [*Miller et al.,* 2007]. Thunderstorms are prevalent in the afternoon over the Al Hajar Mountains and haboob events are commonplace-particularly at the SMART site. Because these thunderstorms form to the east of the SMART site, and the afternoon sun was in the west, clouds did not usually obscure the sun photometer view of the solar disc.

Depending on where exactly an AERONET site was located, the mesoscale circulations of the southern Arabian Gulf region left its signature on the heterogeneous aerosol mixture. The diurnal patterns of Angstrom exponent vary considerably for sites in similar environments. For example the diurnal cycle of α is very large at Al Qlaa with a range of 0.18 (average is 0.77) and a clear pattern of maximum at local noon and minima in the early morning and late afternoon. This pattern contrasts with the diurnal cycle at MAARCO, also a coastal site, which shows a much smaller range, ~0.07, and with nearly the opposite diurnal pattern. The inland desert site of

Hamim had the smallest diurnal range of α (~0.03), and this site also had a small diurnal range in AOD, also ~0.03. This interior desert site was rarely influenced by the sea breeze or by haboobs.

3.1.3 Regional comparison: Arabian Gulf Coast versus Gulf of Oman Coast

One scientific objective of the UAE2 mission was to understand if aerosol properties transit the Al Hajar mountains in the vicinity of the Strait of Hormuz. Typically, the Strait of Hormuz is a convergence zone of southwesterly winds traveling along the western UAE coast and easterly winds passing through the Gulf of Oman. In particular, do the optical depths and Angstrom exponents share similar characteristics, or are there different aerosol properties on the Gulf of Oman and Arabian Gulf? A comparison of the AOD and Angstrom exponents at Dhadnah, located near the coast of the Gulf of Oman, with Umm Al Quwain near the Arabian Gulf coast are shown in Figure 4. These two sites are nearly at the same latitude, 25.513^0 N and 25.533^0 N (~2 km different in North-South direction) and both are located at relatively low altitude (<82 m) but are separated ~70 km in the east-west direction with a mountain range between them. Daily averages are computed only from observations that are also matched in time by 5 minutes or less between the two sites. For the period June 29 – October 13, 2004, there were 81 days when observations were date and time matched. Scatter plots of daily average matched AOD and Angstrom exponents in Figures 4a and b show that there is relatively high correlation in AOD between the sites (~61% of the variance explained) and even higher correlation in Angstrom exponent (~74% of the variance explained). This suggests that on most of the days in summer 2004 the mountain range in the northern UAE between these sites did not act as a separation barrier for aerosol type, as the aerosol concentrations and size mixture were similar on both sides of the mountains.

3.1.4 Regional comparison: Mountain Ridge Top versus Base Altitude

328 Measurements made at the top of the mountain ridge at Jabal Hafeet at 1059 meters altitude
329 were compared to measurements made at the SMART site in Al Ain at 250 meters altitude in
330 order to investigate the vertical partitioning of AOD in the region, for the time interval August
331 11 - October 3, 2004 (Figure 5). The sites were only ~28 km apart in horizontal distance but
332 differed in altitude by about 800 meters. The AOD (500 nm) at these sites were very highly
333 correlated (r^2=0.85), as expected from their relatively close horizontal proximity. The 500 nm
334 AOD at Jabal Hafeet averaged 75% of the value measured at the SMART site with daily average
335 ratios ranging from 51% to 91% (Figure 5). Therefore, an average of ~25% of the total column
336 aerosol AOD at the SMART site was attributed to the lowest 800 meters above ground level
337 during the measurement period. In the interior desert, afternoon boundary layer heights reached 3
338 km [*Reid et al.*, 2007a]. Above 3km additional aerosol layers exist from long-range transport
339 from Europe, Africa, and Southwest Asia [*Reid et al.*, 2007a].
340 The altitude difference between the desert floor and Jabal Hafeet is similar to the altitude
341 difference across the mountain range separating the low altitude sites of Dhadnah and Umm Al
342 Quwain for a ~70 km north-south saddle between the sites (although farther to the north and
343 south some individual peaks reach 1800 m). Therefore, since ~75% of the AOD occurs above the
344 altitude of the mountain ridge for the measurement period, this may explain the high correlation
345 between these sites separated by the mountains (Figure 4) since the mountain ridge may not act
346 as an effective barrier to advection for most of the aerosol layer.
347 The daily average Angstrom exponent (440-870 nm) between the SMART and Jabal Hafeet
348 sites was also highly correlated (r^2=0.90), with the time period (Aug 11 – Oct 3, 2004) average
349 being 0.54 at Jabal Hafeet and 0.49 at SMART. The range in daily average α differences (Jabal-
350 SMART) from +0.18 to -0.11, with an average difference of 0.05, suggests that there was on

average a slightly higher fraction of the total optical depth in the fine mode particle size range above the altitude of the mountain as compared to the layer between the ground and 800 meters above ground level (consistent with the aircraft observations of Reid et al. [2007a]). A similarly high correlation between column water vapor (r^2=0.89) at these two sites also occurred. The average column water vapor ratio (Jabal Hafeet/SMART) was 0.68 with daily averages ranging from 0.55 to 0.79. Therefore, on average during August 11 – October 3, 2004, a higher percentage of the total column water vapor (32%) occurred in lowest 800-meter layer than did the percentage of the total column aerosol optical depth (25%).

3.1.5 Regional comparison: Relationship between AOD and Columnar Water Vapor

In order to accurately assess the full atmospheric influence on regional radiative forcing it is important to understand the possible relationship between AOD and total column water vapor (CWV). The relationship between AOD(500 nm) and total column water vapor at Hamim is shown in Figure 6. Comparisons are made separately for coarse mode dominated cases (α<0.75) and for fine mode dominated cases (α>0.75). For both fine mode and coarse mode dominated cases, there is an obvious trend of increasing AOD as CWV increases, characterized by similar degrees of correlation (r=0.53 for α<0.75; r=0.55 for α>0.75). The relationship of increasing AOD as CWV increases seems independent of particle type (desert dust dominated or fine mode pollution). Additionally, the RH at this inland desert site was very low: the August-September average during daylight hours was ~36% in 2004, resulting in insignificant humidification growth. Therefore, it seems more likely that major aerosol sources are associated with atmospheric flow over the Arabian Gulf (principal regional source of atmospheric moisture) or that perhaps circulation convergence results in air that has both higher AOD and CWV. Similar correlation between AOD(500) and CWV was found for the Gulf island site of Sir Bu Nuair,

374 although the correlation was higher for the fine mode dominated cases (r=0.65 for α>0.75) than
375 for the desert dust dominated cases (r=0.47 for α<0.75). This suggests that aerosol hygroscopic
376 growth may have a somewhat stronger influence for fine mode dominated events over the warm
377 and humid Arabian Gulf. *Smirnov et al.* [2002b] similarly found increasing AOD(500) as CWV
378 increased over Bahrain (a large island in the Arabian Gulf ~380 km WNW of Sir Bu Nuair) in
379 1998-1999 for measurements made over the entire annual cycle. However for fine mode cases
380 they found a significantly higher correlation (r=0.82) while for coarse mode cases the correlation
381 (r=0.45) was similar to what was observed in the UAE in summer.

382 **3.1.6 Retrieval of Fine Mode Fraction from Spectral AOD**

383 Another sub goal of the UAE^2 mission was to study the fidelity of "fine mode fraction"
384 algorithms. Based on the assumption that aerosol size distributions are bimodal, *O'Neill et al.*
385 (2001, 2003) have developed a spectral deconvolution algorithm (SDA) that utilizes spectral
386 AOD data to infer the component fine and coarse mode optical depths from the total extinction
387 aerosol optical depth. The algorithm also fundamentally depends on the assumption that the
388 coarse mode Angstrom exponent and its derivative are close to zero. The Angstrom exponent α
389 and the spectral variation of α (as parameterized by $\alpha' = d\alpha/d\ln\lambda$) are the measurement inputs to
390 the SDA. These continuous-function derivatives (usually computed at a reference wavelength of
391 500 nm) are derived from a second order fit of $\ln \tau_a$ versus $\ln \lambda$ (*Eck et al.*, 1999). The spectral
392 AODs employed as input to the SDA were limited to the CIMEL wavelengths ranging from 380
393 to 1020 nm.

394 Computed fine mode fractions from the SDA algorithm for the Sir Bu Nuair and Hamim sites
395 for August 1 – October 3, 2004 are shown in Figure 7. These sites were chosen for comparison
396 since their temperatures and relative humidity differ significantly, with lower temperatures and

397 much higher RH over the Sir Bu Nuair Gulf island site and higher temperatures and much lower
398 RH over the Hamim site, located in the desert ~125 km inland from the Gulf. The fine mode
399 fraction of the total aerosol optical depth at 500 nm is plotted as a function of $\alpha_{440\text{-}870}$. It is noted
400 that as α increases the fine mode fraction at Sir Bu Nuair is increasingly higher than at Hamim,
401 although only slightly so. The much higher RH at Sir Bu Nuair is expected to result in significant
402 hygroscopic growth of the fine mode particles since there is a sulfate component to this mode
403 [*Ross et al.,* 2007]. Retrievals of the size distributions from the AERONET data using the
404 *Dubovik and King* [2000] algorithm enhanced for spheroid particle scattering [Dubovik et al.,
405 2006] from these same sites do show somewhat larger fine mode particle radius values at Sir Bu
406 Nuair than at Hamim (see section 3.2). Larger fine mode particles at Sir Bu Nuair than at Hamim
407 is consistent with the larger computed fine mode fractions at Sir Bu Nuair for the same value of
408 α, especially for $\alpha > 0.75$ when fine mode AOD begins to dominate the total AOD. However,
409 differences in the magnitude of absorption between these 2 sites may also contribute to
410 differences in the fine mode fraction as computed by the O'Neill algorithm. Mie calculations
411 show that greater fine mode absorption results in lower values of both α and α' for a fine mode
412 only aerosol case [*Eck et al.,* 2001], as the wavelength dependence of scattering optical depth is
413 greater than for absorption optical depth. Thus greater absorption at Hamim (see section 3.2)
414 may also contribute somewhat to computation of smaller fine mode fraction values than for Sir
415 Bu Nuair from the O'Neill algorithm. Nonetheless, even given some differences in particle size
416 and absorption between these 2 sites, there is only a relatively small difference in computed fine
417 mode fraction for a given α (average fine fraction difference of ~0.02 at α=1.2 and 0.00 at
418 α=0.3), and the relationship of α versus fine mode fraction shown in Figure 7 is very informative
419 in the interpretation of the Angstrom exponent in this region. For example, from Table 2 we see

420 that given the measured ~2 month mean of α at Sir Bu Nuair of 0.77, the O'Neill algorithm
421 computes a mean fine mode fraction of ~48%, while for Hamim with a mean α of ~0.57 the
422 O'Neill computed mean fine mode fraction is ~38%. It is emphasized however that the
423 relationship between fine mode fraction and α shown in Figure 7 is representative only for the
424 Arabian Gulf region, since large differences in α may be caused by differences in fine mode
425 particle size that result from coagulation [*Reid et al.*, 1999] and other particle growth processes.
426 For example, *Eck et al.* (2003) found that $\alpha_{440\text{-}870}$ ranged from ~1.1 to 2.0 for biomass burning
427 smoke (fine mode fraction >0.95) with the lower α values from cases of aged smoke with large
428 size accumulation mode particles.
429 We note that the linear relationship between fine mode fraction and Angstrom exponent is
430 predicted by the bi-modal equation (O'Neill et al., 2003):

$$\eta = \frac{\alpha - \alpha_c}{\alpha_f - \alpha_c}$$

431

$$= \left(\frac{1}{\alpha_f - \alpha_c}\right)\alpha + \left(\frac{-\alpha_c}{\alpha_f - \alpha_c}\right) \qquad (1)$$

432 where α_f and α_c, the Angstrom exponents of the fine and coarse mode, can be considered as
433 (intensive variable) constants for a given fine and coarse mode distribution while α is an
434 extensive variable which varies with the coarse and fine mode loading. Equation (1) re-affirms
435 and formalizes the qualitative explanation given above; an environment where fine-mode
436 particles are typically larger (i.e. such as Sir Bu Nuair) will be characterized by smaller values of
437 α_f and thus larger slope values and slightly smaller intercept values (with $\alpha_c \sim -0.15$ as per
438 *O'Neill et al.*, 2003). This is precisely what the regressions of Figure 7 show. It should be noted
439 that the Angstrom exponent employed in Figure 7 ($\alpha_{440\text{-}870}$) should be α(500 nm) to be coherent

with equation (1). However, one can show that $\alpha_{440\text{-}870}$ can be expressed as an approximate MacLaurin-type series in α and α' at 500 nm [*O'Neill et al.,* 2002]. Since η(500 nm) can also be expressed in terms of α and α' (α_f in equation (1) is a weak function of α and α') it follows that η(500 nm) versus α(400-870) actually produces a scattergram with dramatically less dispersion than η(500 nm) versus α(500 nm). This means that the slope of the scattergram will actually be somewhat less sensitive to the fine mode type but that only robustly systematic differences will be displayed.

3.2 AERONET Retrievals of Size Distributions and Single Scattering Albedo

3.2.1 Comparison of Version 2 versus Version 1 Retrievals

The UAE^2 mission afforded one of the first opportunities to evaluate the AERONET Version 2 almucantar retrievals. First, we consider dust-dominated airmasses. Comparisons of retrievals between Versions 1 and 2 for individual almucantar scans over desert (Hamim) and a dark water Arabian Gulf island site (Sir Bu Nuair) are given in Figure 8 with AOD(440) ranging from 0.44 to 0.92 for all cases shown. All Version 1 retrievals in Figure 8 were made with the spheroid particle shape model, since the Version 2 retrievals were dominated by spheroid-shaped particles (100% spheroids for both dust cases and 84% and 89% spheroids for the fine mode cases). Most cases shown are an average of 2-4 retrievals within a single morning or afternoon, while for some it is a single retrieval. The examples given in Figure 8 are desert dust dominated with low Angstrom Exponent ($\alpha_{440\text{-}870}$), ~0.15 to 0.32. The single scattering albedo (ω_o) retrieved using Version 1 for the dust aerosol in these cases showed relatively weak wavelength dependence and significant differences between the two sites, especially at 440 nm where the discrepancy is ~0.03. For Version 2, the differences in spectral ω_o between sites were relatively small (less than 0.01 at all wavelengths) and the decrease at 440 nm relatively large. The decrease in ω_o at short

463 wavelength visible (< 500 nm) and ultraviolet wavelengths is typical of desert dust absorption for
464 aerosol with an iron mineral component [*Sokolik and Toon,* 1999]. Most desert dust in this
465 region is not likely to be hygroscopic [*Li-Jones et al.,* 1998; *Carrico et al*., 2003]; therefore it
466 would be expected that the absorption properties of the dust would be similar whether measured
467 over the humid Arabian Gulf or over the very dry inland desert. The differences in the Version 1
468 ω_o retrievals over the two sites were likely due to differences in surface reflectance that were not
469 accounted for accurately.

470 Comparison of the Version 1 and 2 size distribution retrievals for these same desert dust
471 cases are shown in Figure 8b. For the Hamim site the Version 1 retrieved size distribution shows
472 a bimodal coarse mode while for Version 2 the coarse mode is uni-modal. This bimodal nature is
473 fairly common in all previous Version 1 retrievals of dust atmospheres [*Reid et al.*, 2003]. But,
474 it is also noted that there is less sensitivity to the size of coarse mode particles, as compared to
475 fine mode size, in the AERONET retrieval since particles that are > 1 micron in radius all exhibit
476 relatively little spectral variation in aerosol optical depth from 440 to 1020 nm, while changes in
477 fine mode size affect both the linear (Angstrom) fit of ln τ_a versus ln λ and the curvature or
478 second order polynomial fit. Therefore determination of particle size for the coarse mode
479 depends almost solely on the angular sky radiance distribution, while for fine mode size particles
480 there is significant additional information in the spectral AOD in addition to the sky radiance
481 distribution.

482 In comparison, Figures 8 c and d present Version 1 and 2 retrievals for almucantar scans
483 where a prominent fine mode was also present. For these scans the Angstrom exponent exceeded
484 unity, 1.04 at Hamim and 1.09 at Sir Bu Nuair. The Version 2 single scattering albedo retrievals
485 for these two sites differ more from each other than the Version 1 retrievals. These differences

may reflect physical differences in aerosol absorption that result from the extreme contrast in relative humidity (RH) between the sites, in conjunction with the presence of hygroscopic fine mode particles [*Ross et al.,* 2007]. The higher Version 2 ω_0 at Sir Bu Nuair would be expected based on the high RH (frequently above 70%) compared to the very dry desert air over Hamim. Comparison of the fine mode size distributions of these cases shows that for both sites there is a shift to somewhat smaller size particles in Version 2 versus Version 1 (especially for the Sir Bu Nuair case), while the volume median radius remained similar for the coarse mode.

For these prominent fine mode cases, the new retrieval also resulted in changes in index of refraction. For the Sir Bu Nuair case, the retrieved real refractive index decreased from 1.44 in Version 1 to 1.37 in Version 2, while for the Hamim case the real refractive index decreased from 1.52 in Version 1 to 1.45 in Version 2. In order to maintain retrieval optical depth, this shift to smaller sizes and indices of refraction must also coincide with a comparable increase in amplitude of the particle size distribution. Two month averages of Version 2 retrievals of ω_o and size distributions for the entire range of measured Angstrom exponents for these same two sites will be discussed later in Section 3.2.3 and are shown in Figures 13 and 14.

From this analysis it is clear that significant differences do exist between the older and newer retrievals. These differences for the most part appear to be traced back to improved surface albedo parameterizations. Indeed, the new Version 2 retrievals of dust aerosol single scattering albedo with much lower values in the blue are much closer to what we would expect [e.g., Sokolik and Toon, 1999; Bergstrom et al., 2002]. For the remainder of this manuscript, all subsequent AERONET inversion results presented are Version 2 results of single scattering albedo and size distributions.

509 **3.2.2. In Depth Analyses of Retrievals for Coarse and Fine Mode Dominated Events**

510 **Coarse Mode Dominated Event – September 22, 2004**

511 On September 22, 2004 the AOD at most sites in the UAE was relatively high and the
512 Angstrom exponent relatively low, thus indicating the dominance of coarse mode size particles.
513 During this event regional winds were low, and it appears that dust generated in the UAE
514 stagnated for several days, before being ventilated on Sept 23rd. Consequently, AODs were
515 regionally high and well spread over the region. For this event we compare AERONET
516 almucantar retrievals for four sites spanning the UAE on this date: Dhadnah, Hamim, Mezaira,
517 and SMART in Figure 9. The 440 nm AOD for these sites during the times of the retrievals
518 ranged from 0.55 to 0.69 and the 440-870 nm Angstrom exponent ranged from 0.22 to 0.31.
519 These α values correspond to fine mode fractions of the total optical depth of only ~0.24 to
520 ~0.29, as estimated from the O'Neill algorithm (Figure 7). Seven-day back trajectories from the
521 HYSPLIT model [*HYSPLIT4*, 1997] for Hamim (Figure 10a) for the retrieval time on September
522 22 shows mid-boundary layer flow (final altitude 1500 m above ground level at Hamim)
523 originating in Afghanistan and Iran and near surface trajectory coming from the south over the
524 Indian Ocean, then over Oman and Saudi Arabia. The back trajectory for Dhadnah (Figure 10b)
525 shows that the near surface trajectory is mainly over ocean except 6-7 days prior over coastal
526 Somalia, while the trajectories ending at 1500 and 3000 m originate mainly from Iran, southern
527 Pakistan and Turkmenistan.

528 The volume size distributions for the four sites on September 22 are shown in Figure 9a. The
529 coarse mode dominates and the particle size distributions are similar at all four sites, with the
530 computed volume coarse mode median radius ranging from 2.14 to 2.23 μm. The geometric
531 standard deviation (width) of the size distributions also showed little variance among the sites,

532 ranging from 1.70 to 1.84. For long-distance transported Saharan coarse mode dust in Puerto
533 Rico, *Reid et al.* [2003] found a very large range in volume median radius of ~1.25 to 4.5 μm
534 from a variety of in situ measurement techniques. They attributed these differences to various
535 systematic biases for the different techniques. For in situ measurements made at the MAARCO
536 site during UAE^2, Reid et al. [2007b] found volume median radius ranging from 1.63 to 2.28 μm
537 (geometric standard deviation ranging from 1.78 to 2.16), with size differing for the various dust
538 source regions (Northern UAE/Iran, Iraq, Southern Oman/Yemen, local UAE).
539 The retrievals of single scattering albedo for these same retrievals are shown in Figure 9b.
540 The spectral ω_0 are similar at all four sites, especially for Hamim, Mezaira, and SMART which
541 are within ~0.01 of each other for all 4 wavelengths. Although the ω_0 at Dhadnah are ~0.01 to
542 0.02 lower than at the SMART site, these differences are still within the range of uncertainty of
543 the retrievals (~0.03). The lower ω_0 at Dhadnah may be due to real differences in the aerosol
544 absorption (see different near surface trajectories in Figure 10) or possibly due to greater
545 uncertainty in surface albedo. Since Dhadnah is near the coast (~2 km), the specification of the
546 correct surface albedo and BRDF is much more difficult and complex since the surfaces near this
547 site (desert, mountains, and ocean) have very different reflectance magnitudes as a function of
548 solar zenith angle and also extremely different BRDF shapes (forward scatter glint from ocean
549 versus backscatter maximum over land). We combine the mixture of land and ocean surface
550 BRDF values using weighting by the land-ocean percentage and creating a mixture BRDF that
551 does not account for land surface slope effects such as from hills or mountains.
552 At the SMART site, two CIMEL sun-sky radiometers were operated side by side. The
553 retrievals of ω_0 for these 2 CIMELs at SMART agree to within less than 0.01 for all four
554 wavelengths, suggesting consistent instrument performance and calibration accuracy. The size

555 distribution retrievals for the two SMART site instruments show some minor differences in both
556 fine and coarse modes; however, the computed coarse mode median volume radius was very
557 similar for both, 2.21 and 2.23 μm, with similar coarse mode geometric standard deviations also,
558 1.81 and 1.84.

559 **Fine Mode Dominated Event – September 01, 2004**

560 On September 01, 2004 the Angstrom exponents measured at all AERONET sites in the UAE
561 were relatively high and the AOD mostly above the 2-month mean (Figure 3, day 245). We
562 present the results of AERONET almucantar retrievals from 4 sites on September 1 in Figure 11,
563 with one site (Hamim) on August 31 since there were no good retrievals with high α on
564 September 1 at that site. The 440 nm AOD for these sites during the times of the retrievals
565 ranged from 0.50 to 0.82 and the 440-870 nm Angstrom exponent ranged from 1.02 to 1.33.
566 These α values correspond to fine mode fractions of the total optical depth of ~0.57 to ~0.70
567 (relatively high for the UAE), as estimated from the O'Neill algorithm (Figure 7). However,
568 there is still ~30 to 40% coarse mode fraction for these data and therefore the coarse mode still
569 has significant influence on optical properties even during this pollution event.

570 The August 30-September 1 pollution event brought the highest levels of fine mode particles
571 to the UAE during the entire study. Twenty-four hour particulate matter with diameter < 2.5μm
572 ($PM_{2.5}$) concentrations measured at the MAARCO site topped 100 μg m^{-3}. [*Ross et al.*, 2007].
573 The event was a result of a flow reversal, where previously winds were strong southwesterly.
574 Then starting approximately on August 29, winds reversed to the more typical northwesterly
575 monsoonal flow [*Reid et al.,* 2007a]. A consequence was that the air mass reaching the UAE
576 during the event period spent many days over the Arabian Gulf as demonstrated by the
577 HYSPLIT model seven-day back trajectory analysis for Sir Bu Nuair (Figure 12a). For the

578 retrieval time on September 01 the trajectory analysis shows boundary layer flow at all levels for
579 the prior two days to be nearly parallel to and over the Arabian Gulf and adjacent coastal lands.
580 Most petroleum processing sites are located on islands, platforms and coastal regions and
581 produce significant amounts of sulfate-based particles throughout the Arabian Gulf [*Ross et al.*,
582 2007]. Back trajectories for the SMART, Al Khaznah, and Hamim sites on September 1 (August
583 31 for Hamim) also show that air parcels transited over the Arabian Gulf for the prior two to four
584 days on at least one of the three levels. The back trajectory for Dhadnah (Figure 12b) is quite
585 different however, with only the upper-level trajectory (altitude at 3000 m on Sep 1) over the
586 Arabian Gulf for only 1 day and the surface trajectory over the Gulf of Oman for 2 days, and
587 with the flow at all levels directly from the north over Iran for the majority of the seven-day back
588 trajectory. The lower Angstrom exponent at Dhadnah (1.02) compared to a range of 1.22 to 1.33
589 at the other 4 sites is consistent with the longer transport time over land for the Dhadnah air
590 parcels.

591 The retrievals of ω_0 for the 2 CIMEL sun-sky radiometers at SMART agree to within ~0.01 or
592 less for all four wavelengths, again suggesting consistent instrument performance and calibration
593 accuracy. The size distribution retrievals for the two SMART site instruments show some minor
594 differences in both fine and coarse modes; however, the computed fine mode volume radius was
595 very similar for both, 0.160 and 0.162 μm, with nearly the same fine mode geometric standard
596 deviation, 1.46 and 1.47. These differences are insignificant, and attest to the repeatability of
597 retrievals made with co-located instruments.

598 Comparison of ω_o for these five sites (Figure 11b) shows that the three westernmost sites
599 display no significant wavelength dependence while the easternmost sites (Dhadnah and
600 SMART) are characterized by decreasing ω_0 as wavelength increases. The Arabian Gulf island

site (Sir Bu Nuair) has the weakest absorption, which would be consistent with a large fine mode radius (0.161 μm) resulting from hygroscopic growth induced by high humidity. The sites with the lowest ω_0, especially at 440 and 675 nm, are the inland desert sites of Hamim and SMART. Hamim has relatively small particle radius (0.147 μm), while the SMART site has large radius particles (~0.161 μm). Higher column water vapor at the SMART site (3.2 cm) than at Hamim (2.0 cm) suggest different transport pathways. The comparison in Figure 11 suggests relatively large variability in absorption among the five sites on this date (ω_0 range of ~0.04 at 440 nm and ~0.07 at 1020 nm) possibly due to differences in chemical composition of both fine and coarse modes, but also possibly due in part to uncertainty in surface albedo that differs significantly between sites (brighter sandy desert versus darker water surrounding the Arabian Gulf island). However, the uncertainty in surface albedo may be less important since the ω_0 spectral dependencies for dust cases were consistent (Figure 9b).

3.2.3 Size Distributions and Single Scattering Albedo as a Function of Angstrom Exponent

In this section we analyze the average characteristics of the AERONET retrievals of aerosol size distribution and single scattering albedo as they vary over the observed range of Angstrom exponent. Two sites in contrasting environments are analyzed in detail: Hamim located inland in a sandy desert region with low RH and very high surface temperature, and Sir Bu Nuair located on an island in the Arabian Gulf, with very high RH and lower (but still high) surface temperature. All high quality (AERONET Version 2, level 2.0) almucantar retrievals made over the two-month period of August 1 through October 4, 2004 were grouped into eight bins of Angstrom exponent (Figure 13 and 14). For the Hamim site (Figure 13), the analysis includes 26 almucantar retrievals averaged for each Angstrom exponent bin with bin average α ranging from

623 0.19 to 1.10. For the Sir Bu Nuair site (Figure 14), there are 15 almucantar retrievals averaged
624 for each Angstrom exponent bin with average α ranging from 0.32 to 1.25.

625 The fine mode size distribution retrievals at both Hamim and Sir Bu Nuair show trends of
626 increasing radius as Angstrom exponent increases (Figures 13a and 14a). These trends suggest
627 the possibility that fine mode dust particles may be smaller in size than fine mode pollution
628 particles. Few publications have compared or evaluated the size distribution of fine mode dust
629 particles, but a study has shown that fine mode dust particles are generated in dust events by
630 sandblasting processes [*Gomes et al.,* 1990]. However *Reid et al* . [2007a] did not detect a strong
631 submicron dust mode with surface in situ measurements at MAARCO during the UAE^2
632 campaign, except for very small fine dust (radius ~0.125 μm) originating from Iraq. Fine mode
633 optical depth at 500 nm (as estimated from the O'Neill algorithm) for the α bins shown in Figure
634 13 (and Fig. 14) varied from ~0.12 at α=0.20 to ~0.26 at α=1.12 at Hamim (from τ_{f500}~0.16 at
635 α=0.34 to τ_{f500}~0.42 at α=1.21 at Sir Bu Nuair). The concentrations of fine mode particles in
636 most cases were probably too low to result in significant growth by coagulation. Another
637 possible factor in the fine mode size trend is that the small size fine mode particles retrieved for
638 dust dominated cases may result from low sensitivity to the fine mode particles when the coarse
639 mode dominates, and therefore these smaller particle sizes for low α cases may be partly an
640 artifact of the retrieval.

641 For the largest Angstrom exponent bin averages for each site (1.10 at Hamim and 1.25 at Sir
642 Bu Nuair), the peak value in the fine mode size distribution occurred at ~0.135 μm at Hamim
643 and ~0.16 μm at Sir Bu Nuair. This size difference may result from the much higher relative
644 humidity over the Sir Bu Nuair site, which could foster greater hygroscopic growth.

645 The average size distribution retrievals at Hamim suggest that the coarse mode is slightly
646 bimodal at times (Figures 13a). This results from individual retrievals exhibiting a somewhat
647 bimodal coarse mode, rather than averaging of individual uni-modal coarse mode retrievals of
648 two different sizes. However, we do not place much significance or confidence in whether the
649 coarse mode is really bimodal, since the retrievals have less sensitivity to coarse mode particle
650 size in this size range, as compared to fine mode particle size. One of the input data sets to the
651 almucantar inversion, the spectral aerosol optical depth from 440 to 1020 nm, has minimal
652 information on particle size for particles ~1 micron and larger. The Angstrom exponent for super
653 micron coarse mode particles is nearly zero with small spectral variability [*O'Neill et al.,* 2001].
654 The mean volume median radius of the coarse mode at Hamim ranged from ~2.1 to 2.2 μm (~2.2
655 to 2.5 μm at Sir Bu Nuair) with geometric standard deviation of 1.75 to 1.81 (~1.80 to 1.82 at Sir
656 Bu Nuair) for retrievals made during dust dominated events ($\alpha_{440\text{-}870}$<0.4).
657 The variation in aerosol single scattering albedo as a function of the Angstrom exponent is
658 shown for both Hamim and Sir Bu Nuair in Figures 13b and 14b, respectively. Comparison of
659 the spectral ω_o at these sites for the lowest Angstrom exponent bins (α ranging from 0.19 to 0.32,
660 therefore strong dust domination) shows that the values agree with each other to within ~0.01 to
661 0.015 at all wavelengths, well within the uncertainty of the retrievals of ~0.03. Relative spatial
662 homogeneity in average dust absorption properties is to be expected over the UAE desert and the
663 Arabian Gulf since the dust originates from the same or similar source regions and since the most
664 of the mineral dust aerosol is not hygroscopic [*Li-Jones et al.*, 1998;*Carrico et al.*, 2003], and
665 therefore does not change properties as a function of relative humidity. The mean mid-visible
666 (550 nm) single scattering albedo determined from in situ measurements on aircraft flights in
667 elevated dust layers near Korea and Japan was ~0.96 [*Anderson et al.*, 2003], which is similar to

668 the AERONET measured values in the UAE of ~0.94-0.95, interpolated to 550 nm (Figures 13b
669 and 14b).

670 In contrast to spectral ω_o for the low Angstrom exponent bins, there is a significant difference
671 in the magnitude between Sir Bu Nuair and Hamim for the highest Angstrom bins (α=1.25 and
672 1.10 respectively). In the visible wavelengths (440 and 670 nm) the difference is ~0.03, with
673 higher values at Sir Bu Nuair of ~0.945 at 440 nm versus ~0.915 at Hamim. This is consistent
674 with the larger values of fine mode peak radius at Sir Bu Nuair compared to Hamim (as
675 discussed previously), being likely due to hygroscopic particle growth under high relative
676 humidity conditions at Sir Bu Nuair. The location of a petroleum processing complex between
677 Hamim and the Arabian Gulf coast and the location of several island and offshore platform
678 petroleum extraction and processing facilities in the general vicinity of Sir Bu Nuair also
679 presents the possibility that more or less black carbon is emitted in the aerosol mixtures near
680 these two sites, thus contributing to the observed differences in absorption. The same type of
681 analysis for the Mezaira site, located ~55 km west-northwest of Hamim, shows the fine mode
682 dominated ω_o at α=1.10 (average of 24 almucantars) to be similarly spectrally flat and within
683 <0.01 of the values retrieved at Hamim. The average fine mode dominated ω_o at α=1.22 (average
684 of 5 almucantars) at the Umm Al Quwain site located only ~1 km inland from the Gulf also
685 shows nearly spectrally neutral values within <0.01 of the retrievals at Sir Bu Nuair. These
686 comparisons suggest that there is real regional variation in fine mode single scattering albedo
687 with significantly less absorption occurring over the Gulf and coastal regions than over the
688 desert. The relatively wavelength invariant ω_o for the fine mode dominated cases in the UAE
689 contrasts with fine mode spectral dependence retrieved at other AERONET sites in the world,
690 due to a larger fraction of coarse mode particles present in the UAE. Therefore the persistence of

691 coarse mode particles in this region, even during pollution events, results in the longer
692 wavelength AOD being dominated by super micron size dust particles, thus resulting in weaker
693 absorption as wavelength increases. A comparison of the spectral ω_o at several urban regions in
694 the world dominated by fine mode aerosol [*Eck et al.,* 2005] shows that for locations with highly
695 absorbing aerosol (Mexico City, Beijing and the Maldives) the slope as a function of wavelength
696 is the shallowest for Beijing due to the greater fraction of coarse mode particles at that site.
697 Spectrally decreasing ω_o with increasing wavelength for fine mode dominated aerosols (when
698 the coarse mode is not significant) results from a relatively constant imaginary part of the
699 refractive index that is typical of black carbon absorption [*Bergstrom et al.*, 2002; *Eck et al., 2003*].

701 The spectral ω_o measured over Hamim, for all wavelengths except 440 nm, decreased
702 significantly as the Angstrom exponent increased (Figure 13b). This results from mixtures of
703 weakly absorbing coarse mode aerosols with relatively strongly absorbing fine mode aerosol.
704 The total-column radiatively-effective aerosol 'mixtures' may result from different aerosol types
705 being located in layers at different altitudes above the surface as was commonly observed during
706 ACE-Asia [*Schmid et al*., 2003; *Redemann et al,* 2003], mixed fine and coarse mode aerosols
707 present in the same layers, and also possibly from the coating of large dust particles with fine
708 mode black carbon and other species. The aggregation of fine mode black carbon particles on the
709 surface of coarse mode dust was commonly observed in scanning electron microscopy (SEM)
710 images of aerosol samples obtained in South Korea during the ACE-Asia field experiment
711 [*Arimoto et al.,* 2006]. Typically ~15% to 30% of the surface of dust particles they sampled were
712 coated by black carbon, thus most likely increasing absorption and therefore lowering the ω_o. It
713 is not known to what extent this process of dust particle aggregation with fine mode particles

including black carbon occurred in the UAE environment. The 440 nm single scattering albedo at Hamim did not change much (~0.01) as a function of varying Angstrom exponent since the coarse mode dust is relatively strongly absorbing at this wavelength (due to absorption by iron oxides) and similar in magnitude to the ω_o of the fine mode pollution.

3.2.4 Diurnal Trends in Aerosol Absorption

The diurnal variability of aerosol absorption was investigated by *Remiszewska et al.* [2007] using surface based in situ measurements at a coastal site (MAARCO) approximately 60 km northeast of Abu Dhabi. They found a large diurnal cycle in single scattering albedo with an average diurnal range of ~0.08 at 450 nm, a minimum of ~0.88 in early morning and nearly linearly increasing to a maximum of ~0.96 near midnight, during the time period August 27 to September 30, 2004. This daily cycle in aerosol absorption is explained by *Remiszewska et al*. (2007) as being related to the cycle of the sea breeze circulation, which brings in cleaner air during the day while at night the relatively stagnant air allows more absorbing pollutants to accumulate.

Figure 15 presents the column integrated ω_o at 440 nm inferred from AERONET retrievals at MAARCO from August 27 to September 30, 2004 (same time period) for morning and afternoon time periods where the solar zenith angle range in both intervals is 53-77 degrees and $\tau_{a440} > 0.40$. At ~4:00 UTC (8:00 LST) the AERONET retrieval average ω_o at 440 nm is ~0.916 while at ~1230 UTC the column average is ~0.944, or ~0.03 higher. At the surface, the in situ based measurements at the same times were ~0.88 at 4 UTC and ~0.93 at 1230 UTC [*Remiszewska et al.*, 2007], thus exhibiting a larger increase than the column integrated retrievals. This may be the result of greater absorption dynamics in the lower boundary layer and/or greater diurnal range in days with lower AOD since AERONET retrievals are analyzed

737 only for conditions when AOD(440)>0.4 (since uncertainty is higher at low AOD). The
738 AERONET direct sun measurements of Angstrom exponent (440-870 nm) computed from
739 extinction aerosol optical depth (coinciding with the almucantar retrievals) show no significant
740 change between the morning and afternoon, with an average of 0.620 in the morning versus
741 0.605 in the afternoon. This contrasts with the in situ based Angstrom exponent (450-700 nm)
742 computed from scattering coefficients which increased from ~0.85 to ~1.0 for the times of the
743 AERONET retrievals [*Remiszewska et al.,* 2007]. Additionally, the minimum to maximum
744 daytime diurnal cycle in $\alpha_{440\text{-}870}$ from AERONET is ~0.08 at MAARCO (see Figure 3) while for
745 the same time interval (daylight hours) the in situ nephelometer measured 450-700 nm Angstrom
746 exponent range was ~0.25 or a factor of 3 greater [*Remiszewska et al.*, 2007]. This suggests that
747 the diurnal dynamics in aerosol size distribution is dominated by changes in the lower boundary
748 layer. The columnar aerosol optical depth from AERONET measurements (during the
749 almucantar scans with τ_{a440}>0.4) was higher in the morning, 0.59 at 440 nm versus 0.49 in the
750 afternoon, although this ~17% drop in AOD still results in a high column aerosol loading in the
751 afternoon.

752 The same analysis was performed for other AERONET sites during the UAE2 campaign to
753 further investigate the diurnal variability of absorption. The Al Qlaa site which is also on the
754 coast [~200 km west-southwest of Abu Dhabi, in a less industrialized area] showed essentially
755 no difference in morning versus afternoon retrievals of ω_o at 440 nm with averages of 0.940 in
756 the morning versus 0.943 in the afternoon for a different time period, June 23 –August 24, 2004
757 (the instrument was removed on August 25). There is somewhat greater uncertainty in
758 AERONET retrievals of ω_o at coastal sites due to difficulty in accurately characterizing the
759 BRDF of mixed land-ocean scenes and how this changes with solar azimuth; however, this

760 uncertainty and possible bias may be similar for both the MAARCO and Al Qlaa sites. This
761 suggests that differences between the MAARCO and Al Qlaa sites were real and thus the
762 proximity of the urban plume from Abu Dhabi to the MAARCO site may have contributed to the
763 significant diurnal variation in absorption at that site, which may not necessarily be
764 representative of other coastal sites in the region. There was also no significant diurnal variation
765 (<0.01) in AERONET retrieved ω_o at the inland desert site of Hamim or the Arabian Gulf island
766 site of Sir Bu Nuair (for observations where AOD(440)>0.4) during the months of August
767 through September 2004. Diurnal cycles in absorption would be less likely at these locations due
768 to the lack of significant influence of diurnal sea breeze and land breeze circulations.

769 **4. Summary and Conclusions**

770 The United Arab Emirates Unified Aerosol Experiment (UAE^2) field campaign was
771 conducted in the summer of 2004 (primarily August and September) in order to characterize
772 aerosol properties in the region and to improve aerosol remote sensing over high reflectance
773 surfaces. As a component of this experiment a mesoscale network of 14 AERONET sun-sky
774 radiometers was installed in the UAE and adjacent Arabian Gulf waters. The principal findings
775 of the analyses of these measurements are given below.

776 1. The aerosol loading in the southern Arabian Gulf and UAE region in August-September
777 2004 was high with τ_{a500} averaging from 0.40 to 0.53 over several sites. However, there
778 was significant temporal variability, with daily average τ_{a500} ranging from <0.2 to >1.0
779 and also in daily average $\alpha_{440\text{-}870}$, with extreme values ranging from <0.2 to >1.5. The
780 two-month average $\alpha_{440\text{-}870}$ ranged from 0.77 over Arabian Gulf island sites, to 0.64 at
781 coastal sites, and 0.50-0.57 at inland desert sites. The average fine mode fraction (as
782 computed from the O'Neill et al. algorithm) corresponding to these $\alpha_{440\text{-}870}$ values was

783 ~48% on the Gulf island sites versus ~35% in the inland desert sites. The higher $\alpha_{440\text{-}870}$
784 over Gulf sites results from the majority of the petroleum extraction and processing
785 industries being located on islands, offshore platforms, and coastal locations, while the
786 primary sources of the coarse mode aerosols are in the inland desert regions.
787 2. Two sites (Umm Al Quwain and Dhadnah) located at nearly the same latitude and 70 km
788 apart east-west, but separated by a mountain range, were compared. One site was located
789 on the Arabian Gulf coast while the other was near the Gulf of Oman. Time matched
790 observations showed that there was high correlation in both τ_{a500} (r^2=0.61) and $\alpha_{440\text{-}870}$
791 (r^2=0.74), thereby suggesting that in most cases the Al Hajar mountain range does not act
792 as a barrier to aerosol advection. Comparison of τ_{a500} at two other sites located 28 km
793 apart but differing in altitude by 800 meters showed that on average ~75% of the total
794 column aerosol loading was located above the lowest 800 meter layer. Since the
795 mountain range separating the sites on the Arabian Gulf and the Gulf of Oman is of a
796 similar altitude, this suggests that the aerosol layer is much thicker than the mountain
797 range height and thus there is relatively little blockage by the mountains.
798 3. Average diurnal variability of τ_{a500} varied widely between sites, with the largest diurnal
799 changes occurring at some coastal sites and island sites (probably associated with land
800 breeze/sea breeze circulation) however one inland site near the mountains exhibited a
801 large increase in the late afternoon, possibly due to the influence of haboob winds
802 associated with thunderstorms. The diurnal variation of $\alpha_{440\text{-}870}$ was also largest for some
803 coastal and island sites, again likely due to land breeze/sea breeze circulation.
804 4. Aerosol optical depth increased as total column water vapor increased at both inland
805 desert sites and coastal sites, with correlation coefficients ranging from ~0.45 to ~0.65.

806 This trend occurs for both fine and coarse mode dominated aerosol cases suggesting that
807 major aerosol sources are associated with transport over the humid Gulf and also possibly
808 from haboob-generated dust associated with thunderstorm activity that occurs when
809 column water vapor is high.

810 5. Version 2 almucantar retrievals of aerosol single scattering albedo show significant
811 differences compared to Version 1 retrievals. These differences are likely due primarily
812 to more accurate estimates of surface reflectance. For example, in Version 1 the ω_0 for
813 dust aerosol over a Gulf island site and over a bright desert site differ significantly
814 (~0.03) and show little spectral variation. However, in Version 2 the retrievals for these
815 same scans show very good agreement (differences <0.01) and also significant increases
816 in absorption at 440 nm, which is typical of dust with iron content. These comparisons
817 suggest significant improvement in the Version 2 retrievals of absorption.

818 6. During pollution events when fine mode particles dominated ($\alpha_{440\text{-}870} > 1$), the average
819 retrieved peak volume fine mode particle radius was larger over a Gulf island site
820 (~0.160 μm) than over a desert site (~0.135 μm), which was probably due to hygroscopic
821 growth in the high RH marine environment. Coincident with the particle growth at the
822 marine site is higher single scattering albedo over the Gulf for the pollution-dominated
823 events (~0.03) than at the desert site.

824 7. At an inland desert site (Hamim), the single scattering albedo at 440 nm remains
825 relatively constant (within ~0.01) as a function of Angstrom exponent since both fine and
826 coarse mode particles are absorbing at this wavelength. At longer wavelengths (675 to
827 1020 nm), however, the dust is much less absorbing than the pollution, resulting in
828 differences of ~0.04-0.05 between dust cases with $\alpha_{440\text{-}870} < 0.4$ and pollution cases with

829 $\alpha_{440\text{-}870}$ >1.0. At a Gulf island site (Sir Bu Nuair) there is less contrast in the ω_0 at the
830 longer wavelengths since the pollution aerosol is less absorbing than over the desert.
831 8. At the Gulf coastal site of MAARCO from August 27- September 30, 2004 the aerosol
832 single scattering albedo retrieved from AERONET almucantar scans averaged ~0.03
833 higher in the late afternoon than in the early morning. This is consistent with but less than
834 the ~0.05 greater afternoon ω_0 measured in situ at the surface at this same site and times.
835 This diurnal change is likely related to the land breeze/ sea breeze diurnal cycle, with
836 more absorbing pollution aerosol building up over night and aerosol of a more weakly
837 absorbing nature being advected inland during the day with the sea breeze. However,
838 another AERONET coastal site in a more rural location does not show any diurnal
839 variation in retrieved ω_0 thus suggesting that this dynamic may result from MAARCO
840 being located in a relatively highly industrialized section of the Gulf coast.
841
842
843 **Acknowledgements.** This project was supported by Michael D. King, NASA EOS project
844 office. We thank the staff at the UAE Department of Water Resources (DWRS) directed by
845 Abdulla Al Mangoosh for extensive assistance in all aspects of this field campaign. Steve
846 Braccardo (University of Witwatersrand, South Africa) was responsible for the UAE^2 field
847 campaign project management. We also thank the anonymous reviewers for comments that
848 resulted in improvements in the paper.

References

Anderson, T.L., S.J. Masonis, D.S. Covert, N.C. Ahlquist, S.G. Howell, A.D. Clarke, and C.S. McNaughton, Variability of aerosol optical properties derived from in situ aircraft measurements during ACE-Asia, J. Geophys. Res., 108 (D23), 8647, doi:10.1029/2002JD003247, 2003.

Arimoto et al., 2006, Characterization of Asian Dust during ACE-Asia, Global and Planetary Change, 52, 23–56.

Bergstrom, R.W., P.B. Russell, P. Hignett, Wavelength dependence of the absorption of black carbon particles: Predictions and results from the TARFOX experiment and implications for the aerosol single scattering albedo, J. Atmos. Sci., 59, 567-577, 2002.

Carrico, C.M., P. Kus, M.J. Rood, P.K. Quinn, and T.S. Bates, Mixtures of pollution, dust, sea salt, and volcanic aerosol during ACE-Asia: Radiative properties as a function of relative humidity, J. Geophys. Res., 108 (D23), 8650, doi:10.1029/2003JD003405, 2003.

Cox, C., and W. Munk, 1954: The measurements of the roughness of the sea surface from photographs of the sun's glitter. *J. Opt. Soc. Am.*, **44**, 838-850

Dubovik, O., A. Smirnov, B. N. Holben, M. D. King, Y. J. Kaufman, T. F. Eck, and I. Slutsker, Accuracy assessments of aerosol optical properties retrieved from AERONET Sun and sky-radiance measurements, J. Geophys. Res.,105, 9791-9806, 2000.

Dubovik, O. and M.D. King, A flexible inversion algorithm for the retrieval of aerosol optical properties from Sun and sky radiance measurements, J. Geophys. Res.,105, 20673-20696, 2000.

Dubovik, O., B.N. Holben, T.F. Eck, A. Smirnov, Y.J. Kaufman, M.D. King, D. Tanre, I. Slutsker, Variability of absorption and optical properties of key aerosol types observed in worldwide locations, J. Atmos. Sci., 59, 590-608, 2002.

Dubovik, O. et al., 2006: Application of spheroid models to account for aerosol particle nonsphericity in remote sensing of desert dust. *J. Geophys. Res.*, **111**, doi:10.1029/2005JD006619.

Eager R. E., S. Raman, D. Westphal, J. S. Reid, and A. Al Mandoos, 2007, A Climatological Study of the Sea and Land Breezes in the Arabian Gulf Region, submitted to J. Geophys. Res.

Eck, T.F., B.N. Holben, J.S. Reid, O. Dubovik, A. Smirnov, N.T. O'Neill, I. Slutsker, and S. Kinne, Wavelength dependence of the optical depth of biomass burning, urban, and desert dust aerosols, J. Geophys. Res., 104, 31,333 -31,349 , 1999.

Eck, T.F., B.N. Holben, D.E. Ward, O. Dubovik, J.S. Reid, A. Smirnov, M.M. Mukelabai, N.C. Hsu, N.T. O'Neill, and I. Slutsker, Characterization of the optical properties of biomass burning aerosols in Zambia during the 1997 ZIBBEE Field Campaign, J. Geophys. Res., 106, 3425-3448, 2001.

Eck, T.F., B.N. Holben, J.S. Reid, N.T. O'Neill, J.S. Schafer, O. Dubovik, A. Smirnov, M.A. Yamasoe, and P. Artaxo, High aerosol optical depth biomass burning events: A

comparison of optical properties for different source regions, Geophys. Res. Lett., 30 (20), 2035, doi:10.1029/2003GL017861, 2003.

Eck, T.F., B.N. Holben, O. Dubovik, A. Smirnov, P. Goloub, H.B. Chen, B. Chatenet, L. Gomes, X.Y. Zhang, S.C. Tsay, Q. Ji, D. Giles, and I. Slutsker, Columnar aerosol optical properties at AERONET sites in central eastern Asia and aerosol transport to the tropical mid-Pacific, *J. Geophys. Res.*, **110** , D06202, doi:10.1029/2004JD005274, 2005.

Gomes, L., G. Bergametti, G. Coude´-Gaussen, and P. Rognon (1990), Submicron desert dusts: A sandblasting process, *J. Geophys. Res., 95*, 13,927– 13,935.

Holben, B.N., T.F. Eck, I. Slutsker, A. Smirnov, A. Sinyuk, J. Schafer, D. Giles, and O. Dubovik, AERONET's Version 2.0 quality assurance criteria, Remote Sensing of Atmosphere and Clouds, edited by Si-Chee Tsay, T. Nakajima, R.P. Singh, and R. Sridharan, Proc. SPIE Vol. 6408, 64080Q, doi:10.1117/12.706524, 2006.

Holben, B.N. et al., AERONET - A federated instrument network and data archive for aerosol characterization, Remote Sens. Environ., 66, 1-16, 1998.

Hsu N. C. et al., 2007, Deep Blue characterization of dust and pollution aerosols during the UAE2 experiment, submitted to J. Geophys. Res.

HYSPLIT4 (HYbrid Single-Particle Lagrangian Integrated Trajectory) Model, Web address: http://www.arl.noaa.gov/ready/hysplit4.html, NOAA Air Resources Laboratory, Silver Spring, MD, 1997.

Kalnay, E. and Coauthors, 1996: The NCEP/NCAR Reanalysis 40-year Project, Bull. Amer. Meteor. Soc., 77, 437-471.

Li-Jones, X., H. B. Maring, and J. M. Prospero (1998), Effect of relative humidity on light scattering by mineral dust aerosol as measured in the marine boundary layer over the tropical Atlantic Ocean, *J. Geophys. Res.*, 103(D23), 31,113–31,122.

Lucht, W., and Roujean, J. L., 2000, Consideration in parametric modeling of BRDF and albedo from multi-angular satellite sensors observations. Remote Sensing Reviews, 18, 343-379.

Miller S. D., A. P. Kuciauskas, M. Liu, Q. Ji. J. S. Reid, D. W. Breed, and A. Walker, 2007, Haboob Dust Storms of the Southern Arabian Peninsula. Status, submitted to J. Geophys. Res.

Moody, E., G., M. D. King, S. Platnik, C. B. Schaaf, and F. Gao, Spatially complete global spectral surface albedos: Value-added datasets derived from terra MODIS land products, *IEEE Trans. Geosci. Remote Sens.,* 43 (1): 144-158, 2005.

O'Neill, N.T., T.F. Eck, B.N. Holben, A. Smirnov, O. Dubovik, and A. Royer, Bimodal size distribution influences on the variation of Angstrom derivatives in spectral and optical depth space, J. Geophys. Res., 106, 9787-9806, 2001.

O'Neill, N. T., Eck, T. F., Holben, B. N., Smirnov, A.A. Royer, Z. Li, Optical properties of Boreal Forest Fire Smoke Derived from Sunphotometry, J. Geophys. Res., Vol. 107, No. D11, 10.1029/2001JD000877, 2002.

O'Neill, N.T., T.F.Eck, , A.Smirnov, B.N.Holben, and S.Thulasiraman, 2003, Spectral discrimination of coarse and fine mode optical deph, J. Geophys. Res., 108(D17), 4559, doi:10.1029/2002JD002975.

O'Neill, N. T., T.F. Eck, J. S. Reid, A. Smirnov, and O. Pancrati, 2007, Coarse mode optical information retrievable using VIS to SWIR sunphotometry; application to UAE2 data, submitted to J. Geophys. Res.

Redemann, J., S.J. Masonis, B. Schmid, T.L. Anderson, P.B. Russell, J.M. Livingston, O. Dubovik, and A.D. Clarke, Clear-column closure studies of aerosols and water vapor aboard the NCAR C-130 during ACE-Asia, 2001, J. Geophys. Res.,, 108 (D23), 8655, doi:10.1029/2003JD003442, 2003.

Reid, J.S., E. A. Reid, S. Piketh, S. Cliff, A. Al Mandoos, A. Walker, S-C. Tsay, 2007a, Dynamics of Southwest Asian Dust Particle Size Characteristics with Implications for Global Dust Research, submitted to J. Geophys. Res.

Reid, J. S., S. Piketh, R. Burger, K. Ross, T. Jensen, R. Bruintjes, A. Walker, A. Al Mandoos, D. L. Westphal, 2007b, Observations of summertime atmospheric thermodynamic and aerosol profiles of the southern Arabian Gulf, submitted to J. Geophys. Res.

Reid, J.S., T.F. Eck, S.A. Christopher, P.V. Hobbs, and B.N. Holben, Use of the Angstrom exponent to estimate the variability of optical and physical properties of aging smoke particles in Brazil, J. Geophys. Res.,104, 27,473-27,489, 1999.

Reid, J.S., H.H. Jonsson, H.B. Maring, A. Smirnov, D.L. Savoie, S.S. Cliff, E.A. Reid, J.M. Livingston, M.M. Meier, O. Dubovik, S.C. Tsay, Comparison of size and morphological measurements of coarse mode dust particles from Africa, J. Geophys. Res., 8593, 2003.

Remiszewska, J., P. J. Flatau, K. M. Markowicz, E. A. Reid, J. S. Reid, and M. L. Witek, 2007, Modulation of the aerosol absorption and single-scattering albedo due to synoptic scale and sea breeze circulations: United Arab Emirates experiment perspective, J. Geophys. Res., 112 (D5): D05204.

Ross, K. E., S.J. Piketh, J.S. Reid and E.A. Reid, 2007, Fine mode aerosol particles in the Southern Arabian Gulf and United Arab Emirates, submitted to J. Geophys. Res.

Schmid, B., J. Michalsky, R. Halthore, M.Beauharnois, L. Harrison, J. Livingston, P. Russell, B.

Holben, T. Eck, and A. Smirnov, Comparison of Aerosol Optical Depth from Four Solar Radiometers During the Fall 1997 ARM Intensive Observation Period, Geophys. Res. Lett., 26, 2725-2728, 1999.

Schmid, B., D.A. Hegg, J. Wang, D. Bates, J. Redemann, P.B. Russell, J.M. Livingston, H.H. Jonsson, E.J. Welton, J.H. Seinfeld, R.C. Flagan, D.S. Covert, O. Dubovik, A. Jefferson, Column closure studies of lower tropospheric aerosol and water vapor during ACE-Asia using airborne Sun photometer and airborne in situ and ship-based lidar measurements, J. Geophys. Res., 108 (D23), 8656, doi:10.1029/2002JD003361, 2003.

Sinyuk, A., O. Dubovik, B. Holben, T.F. Eck, F-M Breon, J. Martonchik, R. Kahn, D. J. Diner, E. F. Vermote, J-C Roger, T. Lapyonok, and I. Slutsker, 2007, Simultaneous retrieval of aerosol and surface properties from a combination of AERONET and satellite, Rem. Sens. Env., 107, doi:10.1016/j.rse.2006.07.022.

Smirnov, A., B.N. Holben, T.F. Eck, O. Dubovik, and I. Slutsker, Cloud screening and quality control algorithms for the AERONET data base, Remote Sens. Environ., 73, 337-349, 2000.

Smirnov, A., B. N. Holben, T. F. Eck, I. Slutsker, B. Chatenet, and R. T. Pinker, 2002a: Diurnal variability of aerosol optical depth observed at AERONET (Aerosol Robotic Network) sites, *Geophys. Res. Lett*. , **29** (23), 2115, doi:10.1029/2002GL016305.

Smirnov, A., B.N. Holben, O. Dubovik, N.T. O'Neill, T.F. Eck, D.L. Westphal, A.K. Goroch, C. Pietras, and I. Slutsker, 2002b, Atmospheric aerosol optical properties in the Persian Gulf, J. Atmos. Sci., 59 (3), 620-634.

Sokolik, I.N. and O.B. Toon, Incorporation of mineralogical composition into models of the radiative properties of mineral aerosol from UV to IR wavelengths, J. Geophys. Res.,104 (D8), 9423-9444, 1999.

Volten H., Mu–oz, O., Rol E., de Haan J., F., Vassen, W., Hovenier, J.,W., Muinonen, K., Nousiainen T. (2001), Scattering matrices of mineral particles at 441.6 nm and 632.8 nm. *J. Geophys. Res*., 106, 17375-17401.

Figure Captions

Figure 1. Location of AERONET sites in the UAE and southern Arabian Gulf during the UAE^2 field campaign during the summer of 2004.

Figure 2. Time series of daily averages of aerosol optical depth (500 nm) and Angstrom exponent (440-870 nm) from August 9 through October 2, 2004, for 3 sites in the UAE and one in the adjacent Arabian Gulf.

Figure 3. Mean diurnal variability of aerosol optical depth (500 nm) and Angstrom exponent (440-870 nm) expressed as departures from the daily mean versus hour of the day.

Figure 4. a.) Relationship between AOD (500 nm) at Umm Al Quwain versus Dhadnah, two sites separated by a mountain range, at the same latitude but ~70 km apart in east-west direction. b.) Same as in a.), but for the Angstrom exponent (440-870 nm).

Figure 5. Ratio of AOD at the Jabal Hafeet site to the AOD at the SMART site, showing that over this time period (Aug 11 – Oct 3, 2004) 25% of the aerosol in the total column was in the layer below 800 meters.

Figure 6. Relationship between aerosol optical depth and total column precipitable water at Hamim for instantaneous observations made where a) $\alpha_{440\text{-}870} > 0.75$ and for b.) $\alpha_{440\text{-}870} < 0.75$.

Figure 7. Fine mode fraction, computed from the O'Neill algorithm, versus measured Angstrom exponent ($\alpha_{440\text{-}870}$) at Hamim and Sir Bu Nuair for August 1 – October 2, 2004. Data were screened to remove observations with missing or bad temperature measurements, since at 1020 nm the detector is temperature sensitive, affecting the 1020 nm τ_a.

Figure 8. Comparison of Version 1 versus Version 2 AERONET almucantar retrievals of single scattering albedo and aerosol size distributions for desert dust cases (a. and b.), and for fine mode pollution dominated cases (c. and d.).

Figure 9. Comparison of AERONET retrievals of size distributions and single scattering albedo made at four different sites during a desert dust event on September 22, 2004.

Figure 10. Seven day back trajectories computed from the HYSPLIT model for September 22, 2004 (same date and times as data shown in Figure 9) for the Hamim site (a) and for the Dhadnah site (b).

Figure 11. Comparison of AERONET retrievals of size distributions and single scattering albedo made at five different sites during a pollution event on September 01, 2004 (August 31 for Hamim).

Figure 12. Seven day back trajectories computed from the HYSPLIT model for September 01, 2004 (same date and times as data shown in Figure 11) for the Sir Bu Nuair site (a) and for the Dhadnah site (b).

Figure 13. Average size distributions and single scattering albedos as a function of Angstrom exponent ($\alpha_{440\text{-}870}$) for Hamim for August 1- October 4, 2004 for almucantar scans with $\tau_{a440}>0.4$. There are 26 almucantar scan retrievals averaged for each Angstrom exponent bin.

Figure 14. Average size distributions and single scattering albedos as a function of Angstrom exponent ($\alpha_{440\text{-}870}$) for Sir Bu Nuair for August 1- October 4, 2004 for almucantar scans with $\tau_{a440}>0.4$. There are 15 almucantar scan retrievals averaged for each Angstrom exponent bin.

Figure 15. Morning versus afternoon AERONET retrievals of single scattering albedo (440 nm) at the MAARCO site, for the time interval August 27 through September 30, 2004. Retrievals are made for the same range of solar zenith angles, 50^0 to 77^0, in the morning and the afternoon. Local Time = UTC Time + 3, for comparison to Figure 3.

Table 1. Average surface albedo (solar zenith angle range of 50 to 77) computed from AERONET Version 2 BRDF compared to albedo assumed for all sites in Version 1

Site Name	Albedo 440 nm	Albedo 675 nm	Albedo 870 nm	Albedo 1020 nm
Sir Bu Nuair	0.11	0.12	0.12	0.13
Hamim	0.14	0.47	0.59	0.62
Al Qlaa	0.16	0.29	0.33	0.34
Version 1 – all sites	0.03	0.06	0.20	0.20

Table 2. Average AOD, Angstrom Exp. and Columnar Water Vapor for Aug 9 – Oct 2, 2004

Site Name	Location	500 nm AOD	Angstrom Exponent (440/870 nm)	Water Vapor (cm)
Dalma	Gulf Island	0.44	0.77	2.48
Sir Bu Nuair	Gulf Island	0.49	0.77	3.09
MAARCO	Coast	0.48	0.64	2.75
Umm Al Quwain	Coast	0.53	0.64	3.31
Saih Salam	Coastal Plain	0.49	0.55	2.77
Mezaira	Inland Desert	0.40	0.57	2.32
Hamim	Inland Desert	0.41	0.57	2.47
SMART	Inland Desert	0.43	0.50	2.44

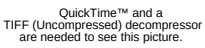

Figure 1. Location of AERONET sites in the UAE and Arabian Gulf during the UAE^2 field campaign during the summer of 2004.

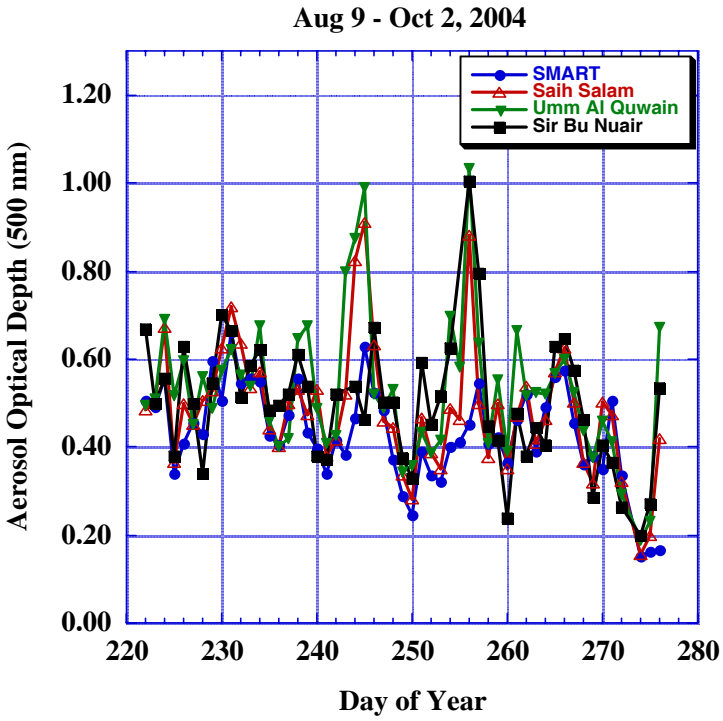

Figure 2a

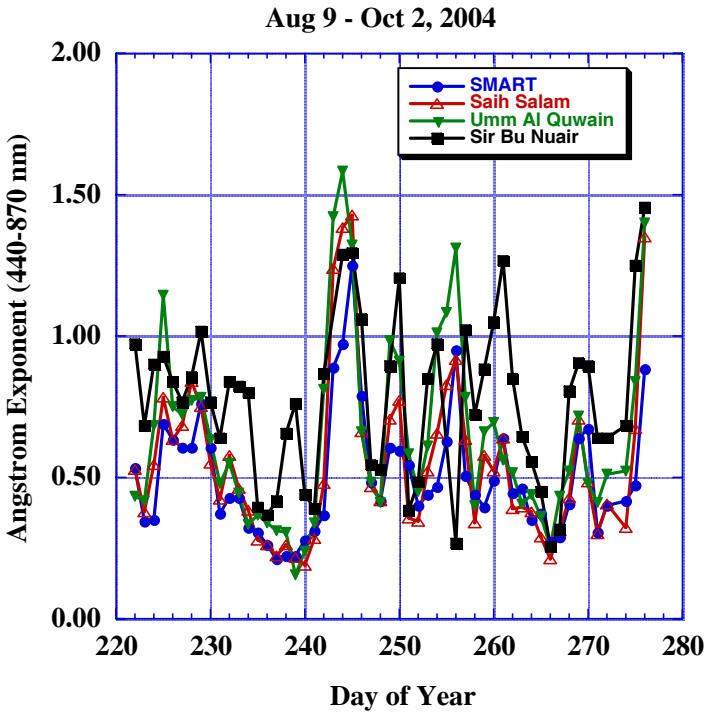

Figure 2b

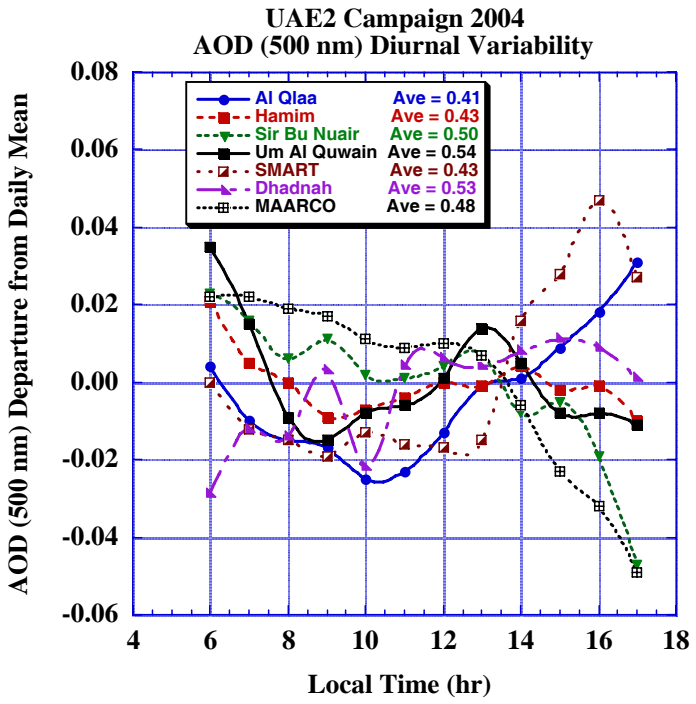

Figure 3a

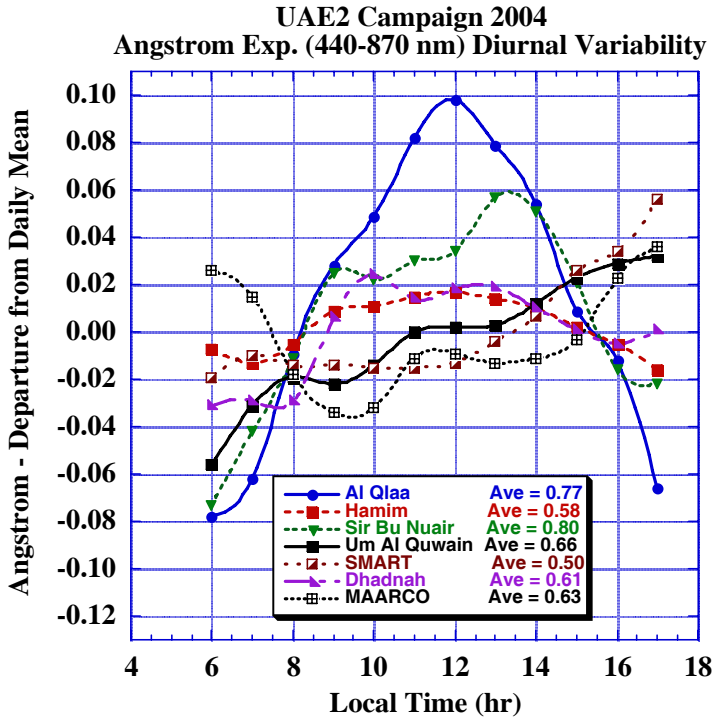

Figure 3b

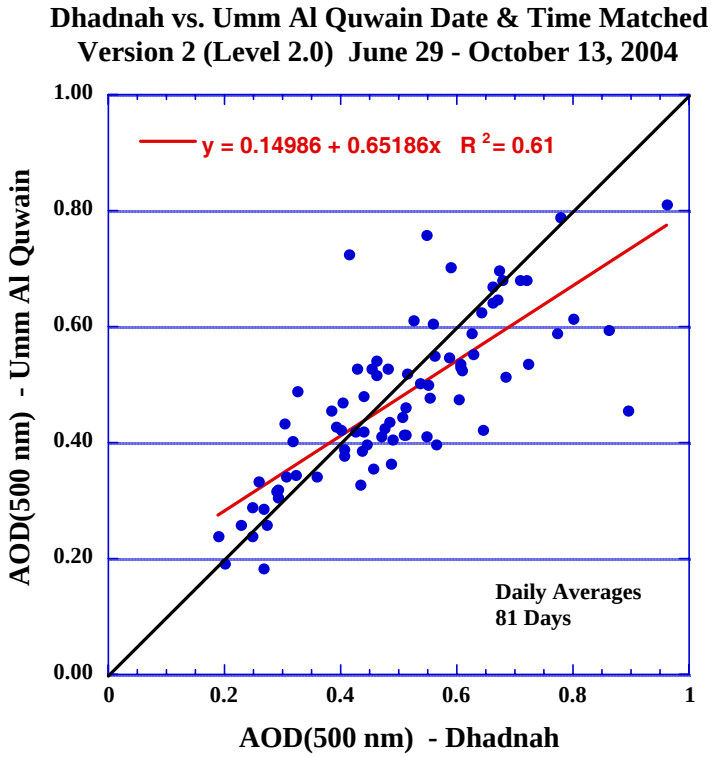

Figure 4a

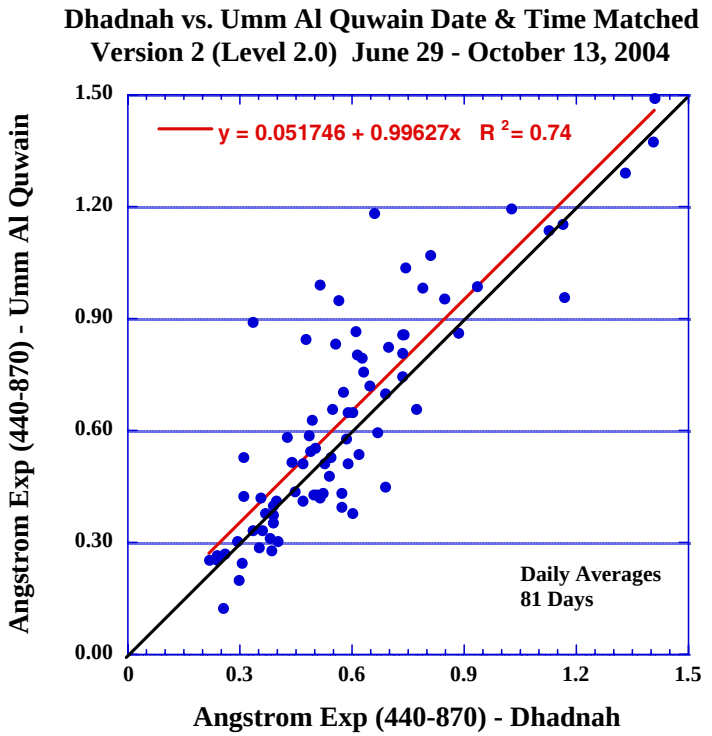

Figure 4b

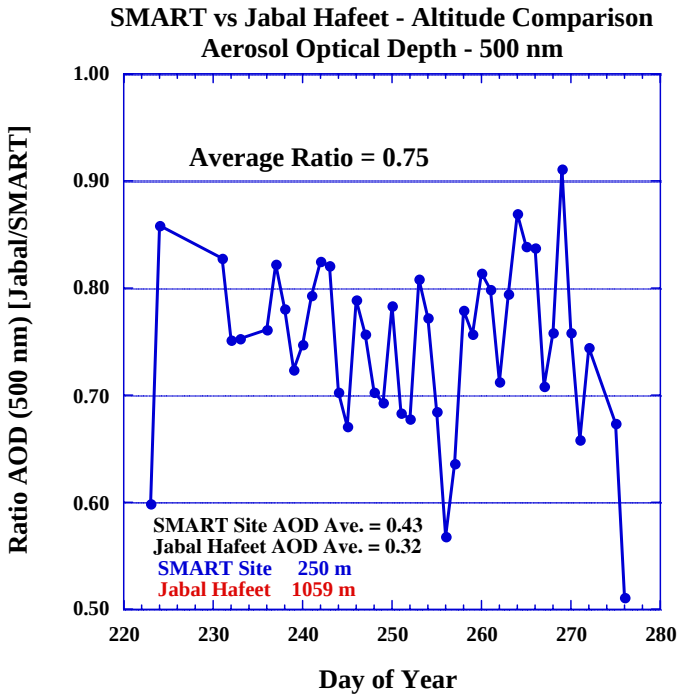
SMART vs Jabal Hafeet - Altitude Comparison
Aerosol Optical Depth - 500 nm
Ratio AOD (500 nm) [Jabal/SMART]
1.00
0.90
0.80
0.70
0.60
0.50
Average Ratio = 0.75
SMART Site AOD Ave. = 0.43
Jabal Hafeet AOD Ave. = 0.32
SMART Site 250 m
Jabal Hafeet 1059 m
220
230
240
250
260
270
280
Day of Year

Figure 5

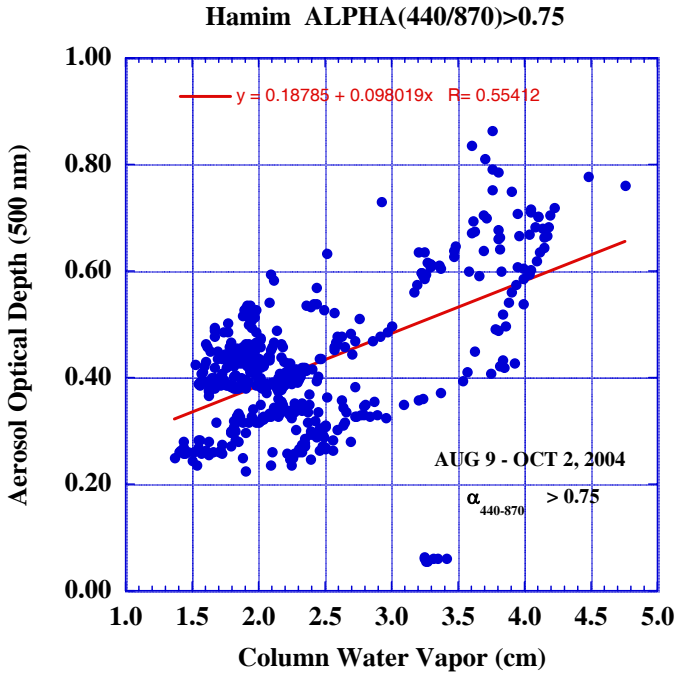

Figure 6a

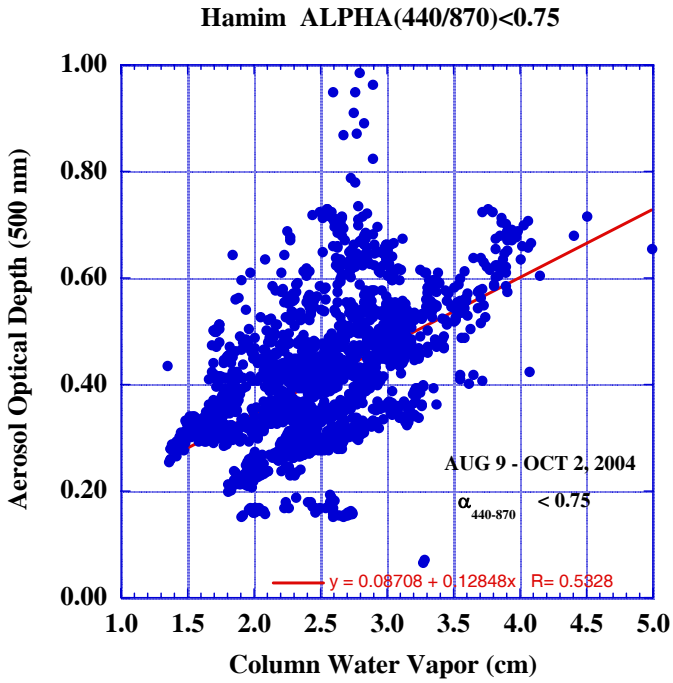

Figure 6b

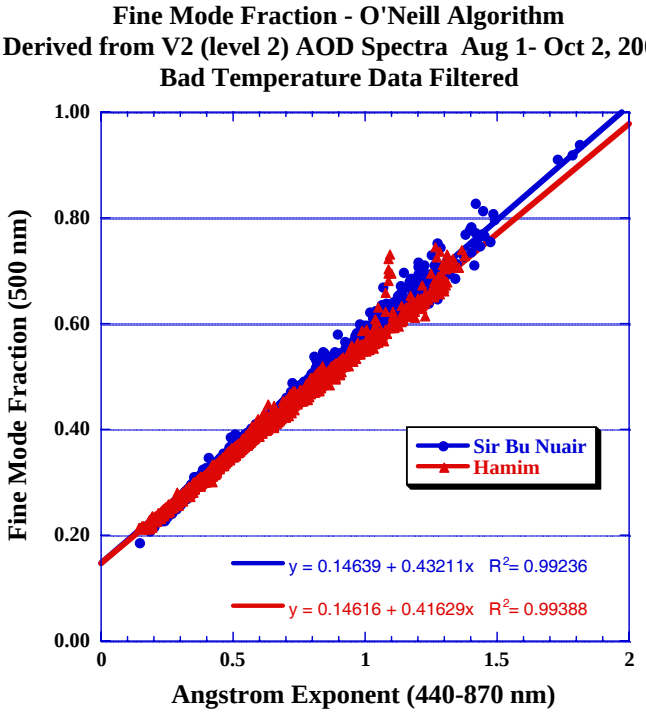
Fine Mode Fraction - O'Neill Algorithm
Derived from V2 (level 2) AOD Spectra Aug 1- Oct 2, 2004
Bad Temperature Data Filtered
Fine Mode Fraction (500 nm)
Angstrom Exponent (440-870 nm)
1.00
0.80
0.60
0.40
0.20
0.00
0
0.5
1
1.5
2
Sir Bu Nuair
Hamim
y = 0.14639 + 0.43211x R2= 0.99236
y = 0.14616 + 0.41629x R2= 0.99388

Figure 7

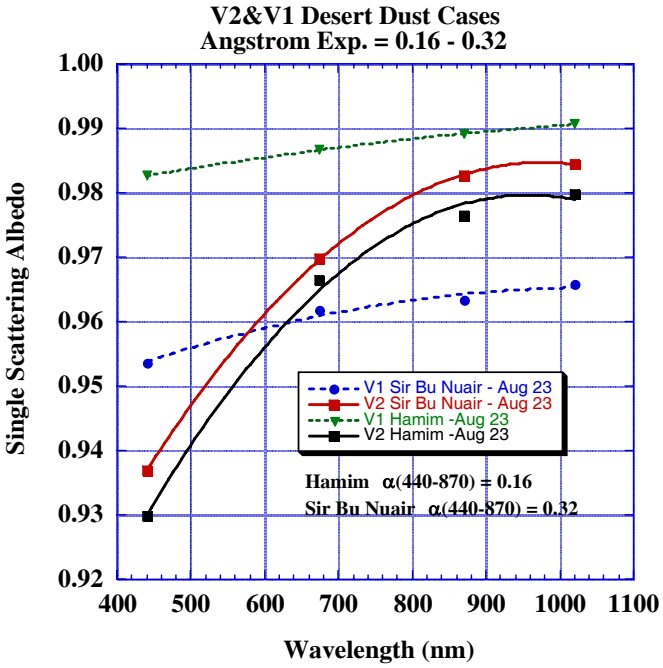

Figure 8a

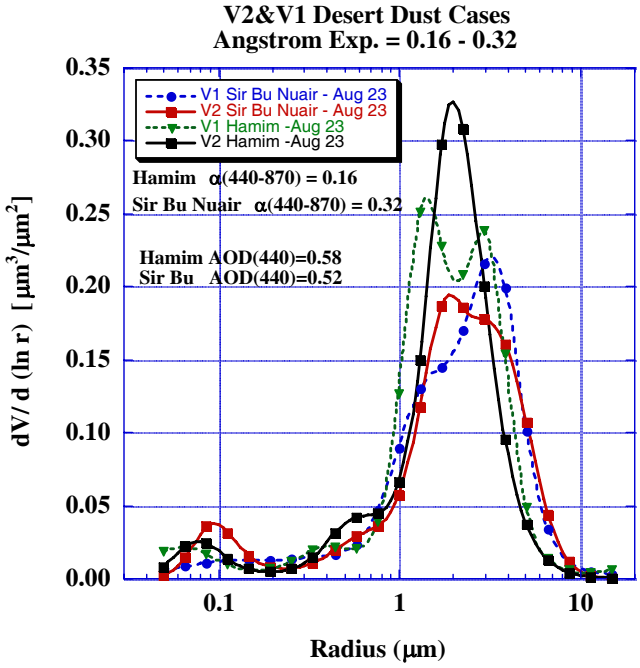

Figure 8b

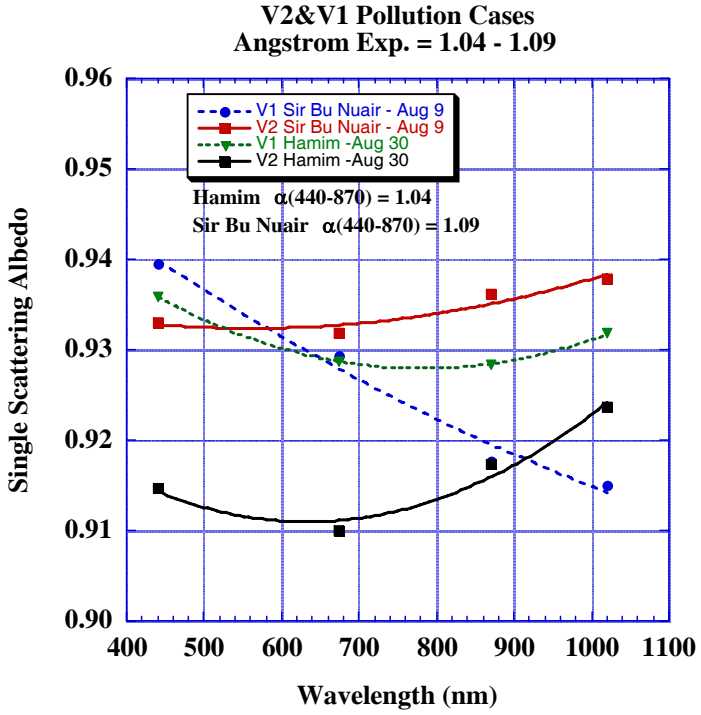

Figure 8c

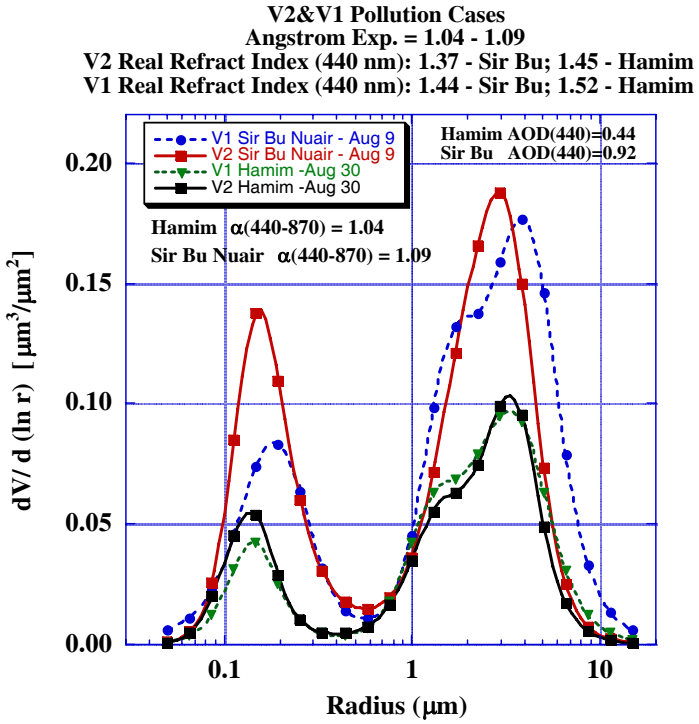

Figure 8d

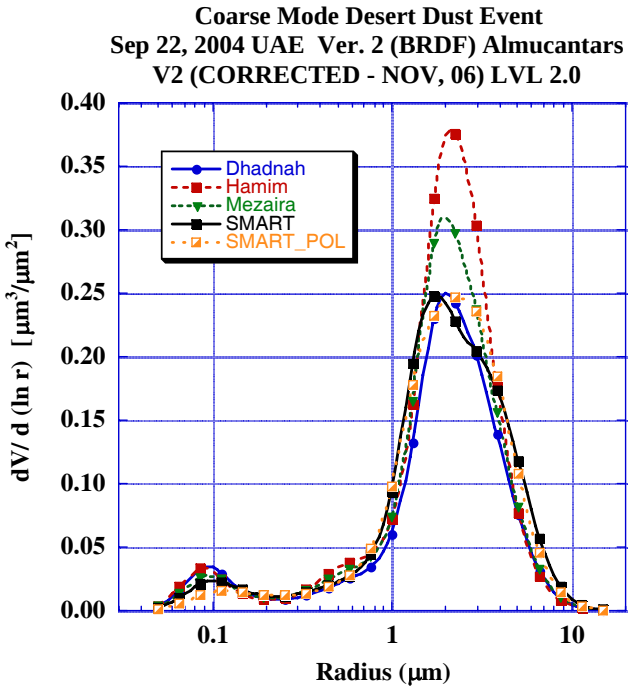

Figure 9a

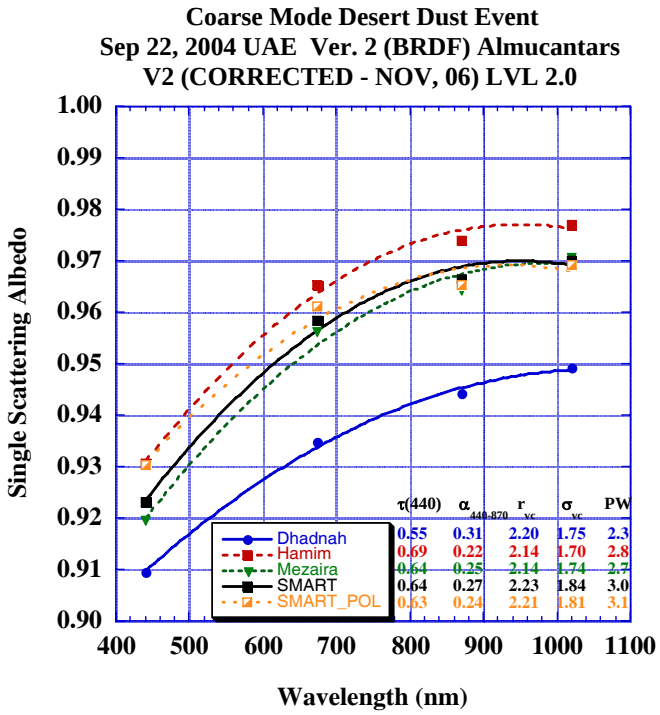

Figure 9b

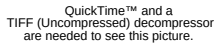

Figure 10a

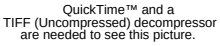

Figure 10b

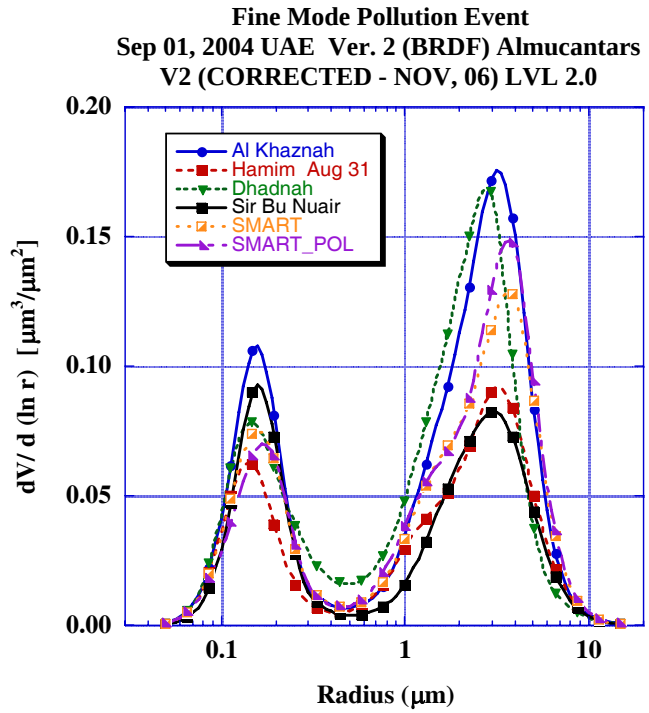

Figure 11a

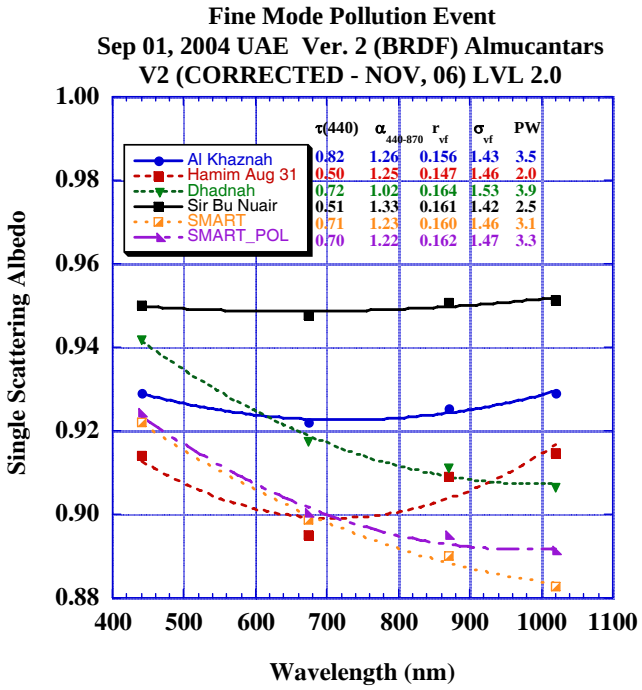

Figure 11b

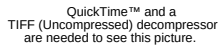

Figure 12a

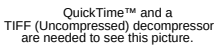

Figure 12b

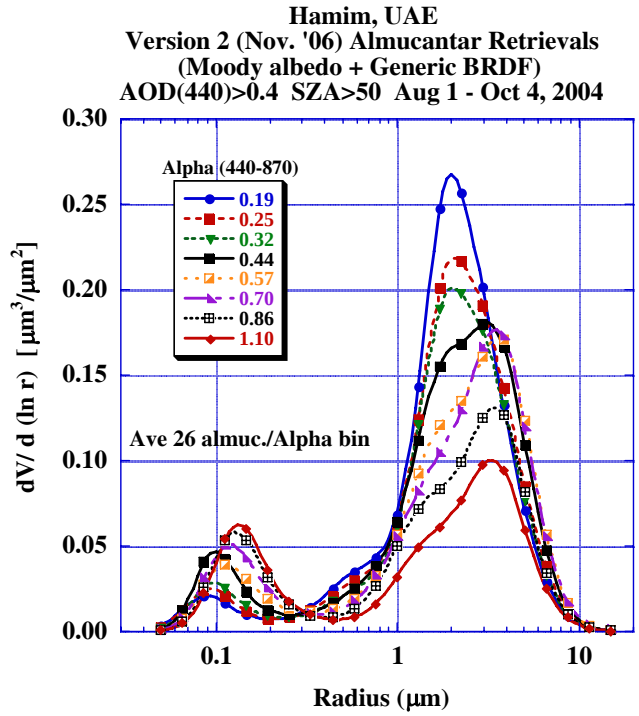

Figure 13a

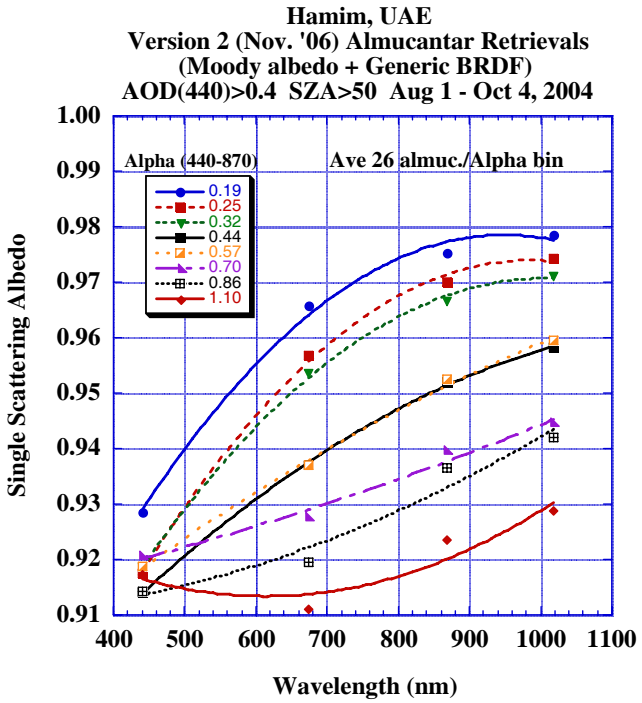

Figure 13b

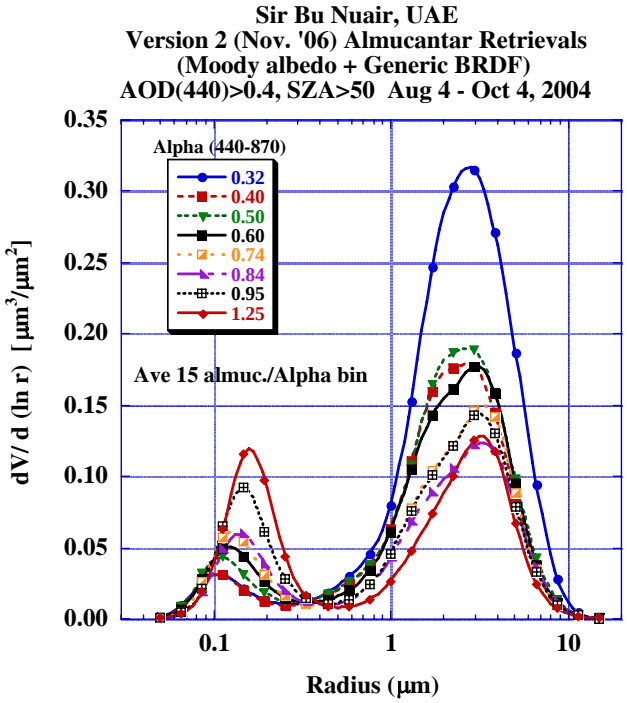

Figure 14a

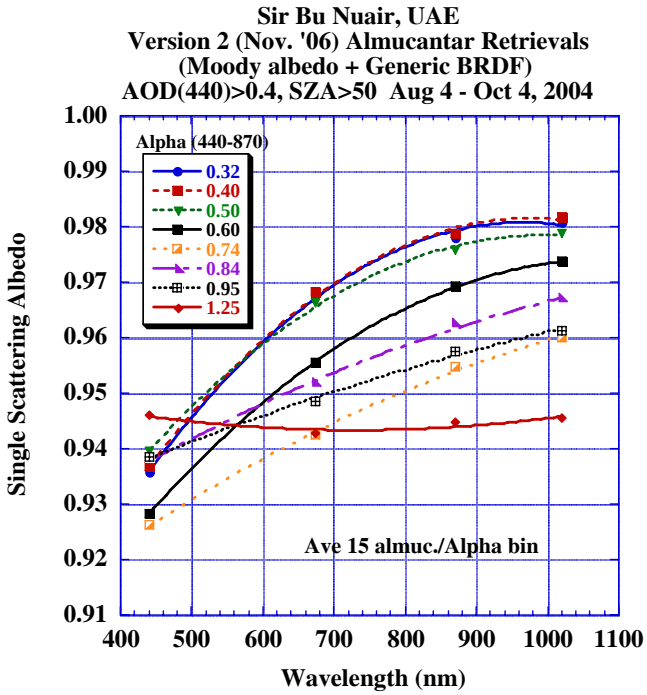

Figure 14b

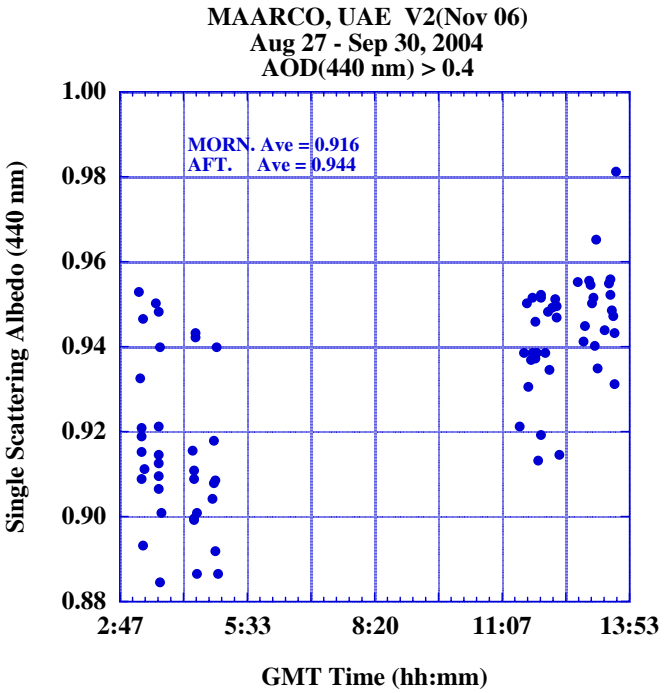
MAARCO, UAE V2(Nov 06)
Aug 27 - Sep 30, 2004
AOD(440 nm) > 0.4
MORN. Ave = 0.916
AFT. Ave = 0.944
Single Scattering Albedo (440 nm)
1.00
0.98
0.96
0.94
0.92
0.90
0.88
2:47
5:33
8:20
11:07
13:53
GMT Time (hh:mm)

Figure 15.